Earth and Planetary Science Letters 482 (2018) 510–524

Contents lists available at ScienceDirect

Earth and Planetary Science Letters

www.elsevier.com/locate/epsl

Cosmogenic signature of geomagnetic reversals and excursions from the Réunion event to the Matuyama–Brunhes transition (0.7–2.14 Ma interval)

Quentin Simon [a,b,*], Didier L. Bourlès [a,1], Nicolas Thouveny [a], Chorng-Shern Horng [c,1], Jean-Pierre Valet [b], Franck Bassinot [d], Sandrine Choy [a,b]

[a] Aix-Marseille Université, CNRS, IRD, Coll France, CEREGE UM34, 13545 Aix en Provence, France
[b] IPGP, Université Paris Diderot, Sorbonne Paris-Cité, UMR 7154 CNRS, 1 rue Jussieu, 75238 Paris, France
[c] Institute of Earth Sciences, Academia Sinica, P.O. Box 1-55, Nankang, Taipei, Taiwan
[d] LSCE, UMR8212, LSCE/IPSL, CEA-CNRS-UVSQ and Université Paris-Saclay, Gif-Sur-Yvette, France

ARTICLE INFO

Article history:
Received 20 June 2017
Received in revised form 12 October 2017
Accepted 10 November 2017
Available online xxxx
Editor: B. Buffett

Keywords:
authigenic $^{10}Be/^{9}Be$ ratios
Matuyama–Brunhes transition
Jaramillo and Olduvai subchrons
Cobb Mountain and Réunion events
Matuyama geomagnetic excursions
lock-in depth

ABSTRACT

Long-term variations of the geomagnetic dipole moment (GDM) during periods of stable polarity and in transitional states (reversals and excursions) provide key information for understanding the geodynamo regime. Following several studies dealing with the Brunhes chron and the Matuyama–Brunhes transition, this study presents a new authigenic $^{10}Be/^{9}Be$ ratio (Be-ratio) record obtained from the MD97-2143 core (western Pacific Ocean). This new Be-ratio series yields a record of GDM variations covering the early Brunhes and mid to late Matuyama time period (i.e. 700–2140 ka), independently from the relative paleointensity (RPI) record obtained from the same core, that can be compared with available RPI records and stacks. Stratigraphic offsets measured between the Be-ratio peaks and the corresponding RPI minima reach 2 to 14 cm. They can be assigned to (post-) detrital remanent magnetization (pDRM) effects leading to magnetization locking-in delays varying from 2 to 12 ka in the studied core. ^{10}Be overproduction episodes triggered by geomagnetic dipole moment lows (GDL) linked to polarity reversals and excursions confirm the global control exerted by the GDM on cosmogenic radionuclides production. A dipole moment reconstruction derived from the Beryllium-10 (BeDiMo) was compiled and calibrated using absolute paleointensity data. This independent record complements the available paleomagnetic RPI records, permitting 1) to overcome the pDRM lock-in offsets induced below the mixing layer, 2) to confront and increase the robustness and precision of GDM reconstructions and, 3) to better constrain the chronology of geomagnetic field instabilities during the mid to late Matuyama chron. Our new ^{10}Be derived inventory is fully compatible with the GDL series linked to geomagnetic polarity reversals and events (Matuyama–Brunhes transition, Jaramillo and Olduvai subchron boundaries, Cobb Mountain, Réunion) and it strengthens the occurrence of several excursions (Kamikatsura, Santa Rosa, Punaruu, Bjorn, Gilsa, Gardar) that were until now reported from only sparse locations.

1. Introduction

Large amplitude departures of the Earth magnetic field from the geocentric axial dipole (GAD) configuration were recorded in geological archives. They correspond to 1) full reversals followed by lasting stable polarity chrons or subchrons, and 2) aborted, i.e. transient or incomplete, reversals called excursions, followed by a re-stabilization in the initial polarity (e.g. Laj and Channell, 2015). The quality and accuracy of transitional paleomagnetic vector directions depend on the geological nature and temporal resolution of the archives, often providing inadequate records for high precision paleo-field reconstructions (e.g. Valet et al., 2016). Simultaneously to these transitional directions, absolute or relative paleointensity (RPI) determinations obtained from lava flows or sediments document systematically the occurrence of geomagnetic dipole moment lows (GDL). The fact that these GDL, either related to polarity reversals or to excursions, reveal similar dynamics (or behavior) (Valet et al., 2005; Ziegler et al., 2011), tends

* Corresponding author at: CEREGE, Europôle Méditerranéen de l'Arbois, BP80, 13545 Aix-en-Provence, cedex 4, France.
E-mail address: simon@cerege.fr (Q. Simon).
[1] LIA-D3E (International Associate Laboratory – From Deep Earth to Extreme Events), CNRS (France) and Academia Sinica (Taiwan).

https://doi.org/10.1016/j.epsl.2017.11.021

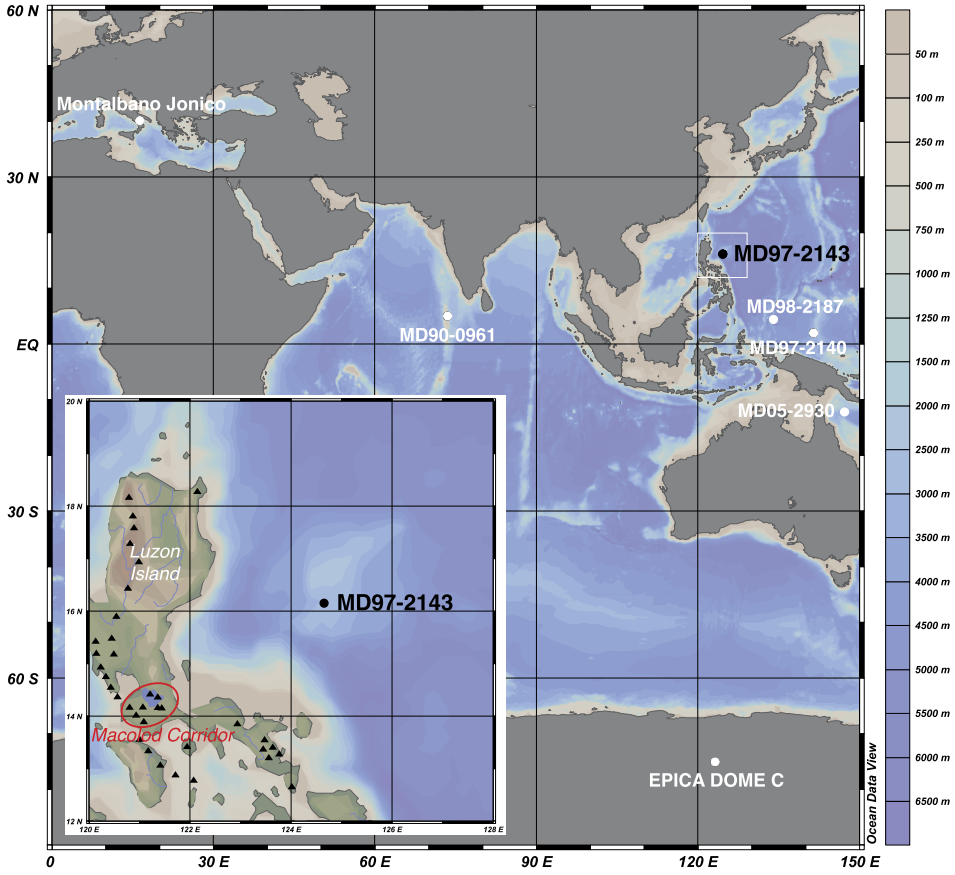

Fig. 1. Location of core MD97-2143 from Benham Rise, western Philippine Sea. Other sites discussed in the text are represented by white dots: MD97-2140 (Carcaillet et al., 2003); MD98-2187 (Suganuma et al., 2010); MD05-2930 (Ménabréaz et al., 2014; Simon et al., 2016a); MD90-0961 (Valet et al., 2014); Montalbano Jonico (Simon et al., 2017); EPICA Dome C (EDC) (Raisbeck et al., 2006). Volcanoes from the Luzon Island are identified by solid triangles.

to suggest that common mechanisms trigger the relevant geodynamo processes. However, the resolution and/or limits of the available paleointensity records result in controversial interpretations and lead to a small number of detailed recordings (Singer, 2014; Valet and Fournier, 2016). Dipole moment reconstructions drawn from multiple proxy-records are thus essential in order to document accurately geodynamo variations, and provide robust constraints to confront numeric or analogic simulations of these processes (e.g. Glatzmaier and Coe, 2015).

The cosmogenic radionuclides (c.n.) atmospheric production inversely proportional to the geomagnetic field intensity constitutes an alternative and complementary approach to classic paleomagnetic measurements for assessing geomagnetic field intensity variations. The theoretical relationships between the geomagnetic dipole moment (GDM) and the rate of c.n. atmospheric production (e.g. Beer et al., 2012 and references therein) supports the methodological grounding to reconstruct GDM variations from c.n. production records in sediment and ice archives. The measurements of beryllium-10 (^{10}Be) content from marine sediments or ice records demonstrated the occurrence of ^{10}Be overproduction episodes associated with GDM collapses synchronous to reversals or excursions (e.g. Raisbeck et al., 2006; Christl et al., 2010; Suganuma et al., 2010; Ménabréaz et al., 2012; Valet et al., 2014; Simon et al., 2017). They also reflect large-amplitude ^{10}Be overproduction series favorably compared to RPI records and stacks (e.g. Frank et al., 1997; Carcaillet et al., 2003, 2004; Ménabréaz et al., 2014). Recently, Simon et al. (2016a) produced the first compilation extending over the whole Brunhes chron, completing the RPI-based GDM reconstructions and focusing on independent estimates of the amplitude of GDM collapses associated with the Matuyama–Brunhes polarity transition (MBT) and Brunhes excursions.

The present study provides new authigenic ^{10}Be/^{9}Be ratio (Be-ratio hereafter) results obtained over the 0.7–2.14 Ma time interval from core MD97-2143 (Horng et al., 2002, 2003). With a long and continuous oxygen isotope record and a robust RPI series integrated in most of the RPI stacks (SINT-2000, PISO-1500, PADM2M), this core is particularly well-suited to extend the time period covered by former ^{10}Be-derived GDM reconstructions (Simon et al., 2016a). Such an extension supports an accurate inventory useful for geodynamo simulations and for high resolution geochronology of the Plio-Quaternary.

2. Material and methods

2.1. Environmental settings and core description

The CALYPSO giant piston core MD97-2143 was collected during the IMAGES III IPHIS cruise of the French R/V Marion Dufresne at a water depth of 2989 m from the Benham Rise, offshore of the eastern Luzon in the western Philippine Sea (Fig. 1; 15.87°N, 124.65°E). The 3800 cm long core is mainly composed of greyish yellow to yellow orange hemipelagic calcareous nannofossil ooze (i.e. coccolithophore) with intercalated foraminiferal ooze and few tephra layers (Fig. 2g). The depth interval studied for Be-ratio analyses extends from 1470 to 3300 cm where a white foraminiferal sandy layer dominated by reworked fossils marks the base of the paleomagnetic record (Horng et al., 2002). The sediments are homogeneous from 1470 to 2200 cm and interrupted by tephra layers of 2–16 cm thickness between 2210 and

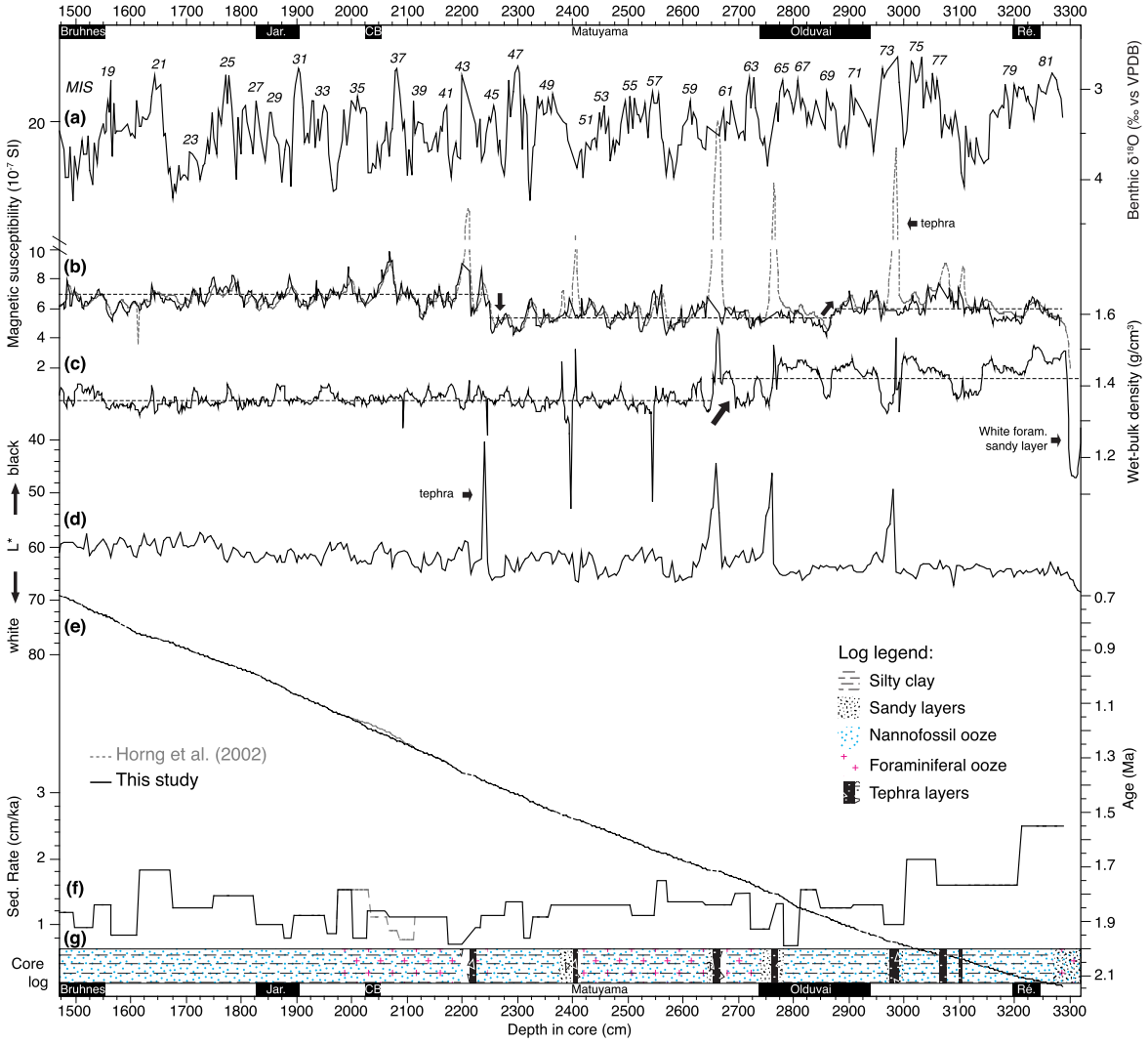

Fig. 2. Chronology and sedimentological description of core MD97-2143. (a) Benthic δ^{18}O (*Cibicides wuellerstorfi*) record (Horng et al., 2002) and marine isotopic stages (MIS). (b) Magnetic susceptibility measured on individual samples (black line) and on the whole core (grey dashed line). (c) Wet-bulk density and (d) sediment lightness (L*). (e) The original ages model of Horng et al. (2002) and its derived sedimentation rates (f) have been slightly adjusted around the MIS 35/36 transition in this study (see text and supplementary Fig. S1). (g) Sediments description is synthesis in a core log based on the IPHIS mission report and physical data.

3106 cm (Fig. 2). The thicker tephra layers were easily identified by high magnetic susceptibilities (Fig. 2b) and low reflectance values (darker color, Fig. 2d). Some of these layers present an upward grading from coarse sand to fine silt suggesting distal turbiditic influences on their deposition mode. The interval characterized by large tephra layers and ubiquitously volcanic ashes dissemination (2200–3100 cm) presents significantly lower average magnetic susceptibility (Fig. 2b), and large density changes below 2650 cm (Fig. 2c).

2.2. Oxygen isotope stratigraphy and core chronology

The oxygen isotope stratigraphy (δ^{18}O) was established by Horng et al. (2002) on the benthic foraminifera *Cibicidoides wuellerstorfi* picked from the >150 μm fraction sampled each 4 cm along the core depth (Fig. 2a). After removal of thick tephra layers (total thickness = 93 cm), an astronomical calibration was achieved by tuning the δ^{18}O record to a target curve using the astronomical solution of Laskar et al. (1993) (see detailed procedure in Horng et al., 2002, 2003). In this study, we carefully compared the δ^{18}O record corrected by +0.64‰ (Shackleton, 1974) with the LR04 stack (Lisiecki and Raymo, 2005) providing strong confidence in the core chronology, except for a ~18 ka offset at the MIS 35/36 transition (see Supplementary Material, Fig. S1). Despite identified regional offsets between benthic series at glacial termination producing stratigraphic misalignments of few ka (Lisiecki and Raymo, 2009), the MD97-2143 δ^{18}O record was correlated to the LR04 stack for this specific interval, leading to a slightly revised chronology (Fig. 2e). This precision is particularly important for interpreting results around 1.2 Ma. Sedimentation rates derived from the age model vary around an average of 1.2 ± 0.3 cm/ka in the studied interval, with maximum values of ~2.0 cm/ka above the reworked foraminiferal sandy layer (3040–3300 cm; >1.994 Ma), implying higher energy at these depths/ages (Fig. 2f).

2.3. Paleomagnetic results

Detailed paleomagnetic and rock magnetic measurements were conducted on 1441 discrete samples by Horng et al. (2002, 2003). Surficial oxidized low-Ti magnetite was identified as the dominant remanent magnetization carrier. Fairly constant rock magnetic properties along the sediment sequence supported the standard quality criteria for RPI reconstruction. This was performed by normalizing the natural remanent magnetization intensity by magnetic susceptibility (Fig. 3e) or isothermal remanent magnetization with consistent results. After checking the absence of lithologi-

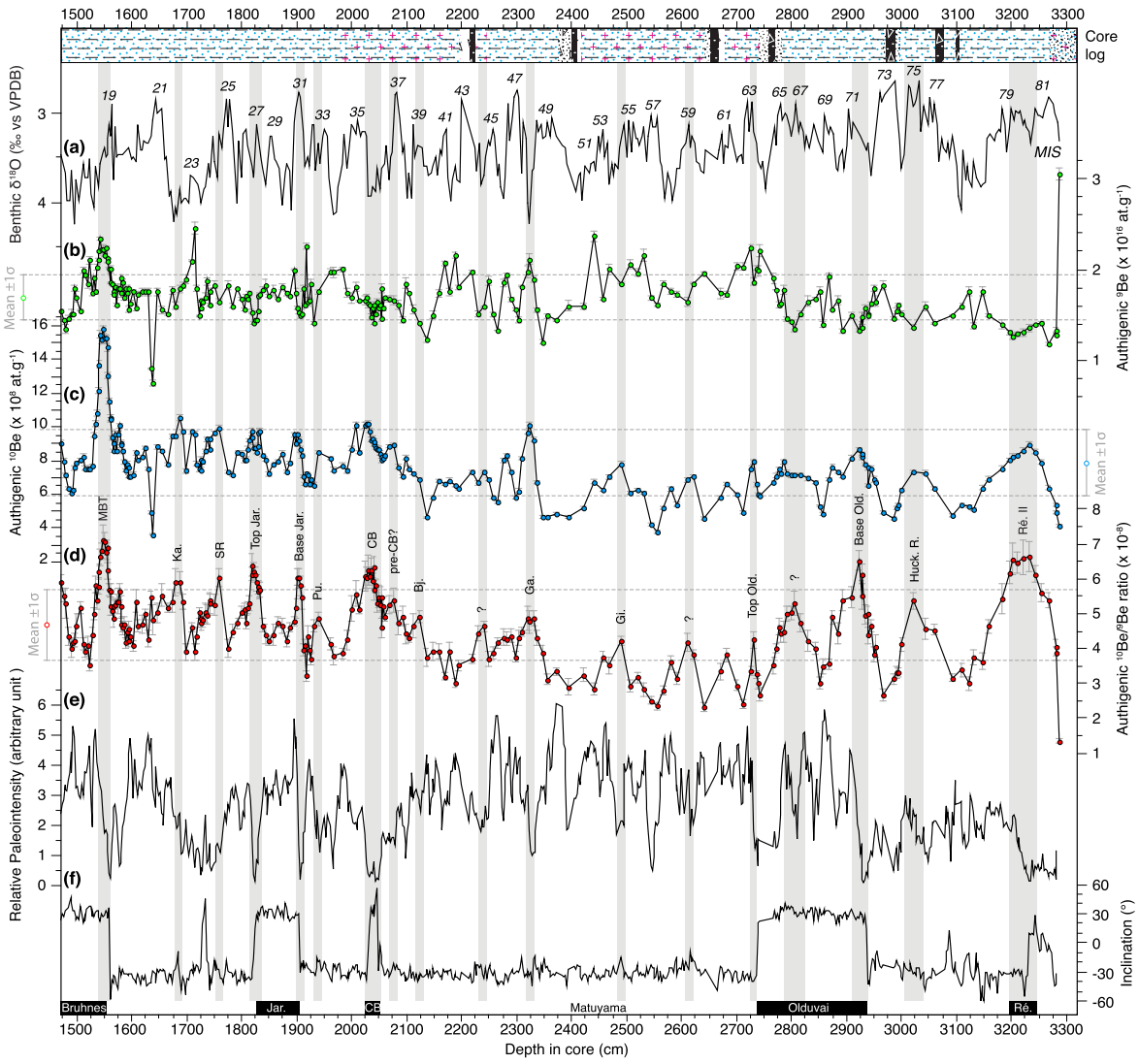

Fig. 3. Paleomagnetic and Be results of core MD97-2143. (a) Benthic $\delta^{18}O$ record. (b) Authigenic ^{9}Be concentration. (c) Authigenic ^{10}Be concentration. (d) Authigenic $^{10}Be/^{9}Be$ ratio (Be-ratio). (e) Relative paleointensity (RPI) and (f) inclination. Geomagnetic events (reversals and excursions) have been labeled and refer to the geomagnetic polarity time scale (bottom): MBT (Matuyama–Brunhes transition), Ka. (Kamikatsura), SR (Santa Rosa), Jar. (Jaramillo), Pu. (Punaruu), CB (Cobb Mnt), Bj. (Bjorn Exc.), Ga. (Gardar Drift), Gi. (Gilsa), Old. (Olduvai), Huck. R. (Huckelbury Ridge), Ré. (Réunion).

cal/environmental contamination, the RPI record was compared to other regional RPI series, and later integrated in several RPI stacks: SINT-2000 (Valet et al., 2005), PISO-1500 (Channell et al., 2009) and PADM2M (Ziegler et al., 2011).

Characteristic remanent magnetization (ChRM) directions were computed in the 15–60 mT alternating field demagnetization range. Maximum angular deviation lower than 5° point out a high accuracy ChRM direction determination for establishment of the magnetic polarity stratigraphy (Fig. 3f). The normal polarity above 1560 cm characterizes the Brunhes chron. Two long-standing normal polarity magnetozones at depth intervals 1824–1904 cm and 2740–2936 cm evidence the Jaramillo and the Olduvai subchrons, respectively. Two thick tephra layers deposited at 2655–2671 cm and 2755–2773 cm however hinder an accurate identification of the upper Olduvai transition (Fig. 3e–f). Three short normal polarity intervals were attributed to the Kamikatsura or Santa Rosa excursions (1729–1734 cm), to the Cobb Mountain (2032–2047 cm) and to the Réunion (3232–3250 cm) geomagnetic events. RPI minima accompanied all reversals, excursions or geomagnetic events (Fig. 3e–f).

2.4. Sample preparation and measurements

The authigenic beryllium isotope analyses were carried out at the CEREGE National Cosmogenic Nuclides Laboratory (LN_2C, France). A total of 250 samples selected with an average 7-cm (~6 ka) resolution were collected from the paleomagnetic cubes and treated according to the chemical procedure established by Bourlès et al. (1989) and summarized by Simon et al. (2016b). The MBT, Jaramillo and Olduvai boundaries and Cobb Mountain events were scrutinized with higher sampling resolution (~2 ka). Authigenic ^{10}Be and ^{9}Be were extracted from each 1 g dry sample by soaking them in 20 ml of 0.04 M hydroxylamine (NH_2OH–HCl) in a 25% acetic acid leaching solution at 95 ± 5°C for 7 h. A 2 ml aliquot of the resulting leaching solution was sampled for the measurement of the natural ^{9}Be concentration which is used as a normalizer to minimize potential environmental disturbances of the ^{10}Be signal (Bourlès et al., 1989). The remaining solution was spiked with 300 µl of a $9.8039.10^{-4}$ $g.g^{-1}$ ^{9}Be-carrier before Be-purification by chromatography in order to accurately determine ^{10}Be sample concentrations from the accelerator mass spectrometer (AMS) measurements of $^{10}Be/^{9}Be$ ratios. The natural authigenic ^{9}Be concentrations were measured us-

ing a graphite-furnace Atomic Absorption Spectrophotometer (AAS) with a double beam correction (Thermo Scientific ICE 3400®). The standard-addition method and the addition of a constant volume of $Mg(NO_3)_2$ solution were used to eliminated the matrix effects during the absorption and to allow measurements near the detection limit. Authigenic ^{9}Be sample concentrations vary around $2.55 \pm 0.39 \times 10^{-7}$ g.g^{-1}. The associated uncertainties (2σ) based on the reproducibility of quadruplicated measurements and the least-square fitting between measured absorbance at each stages of the standard-addition method vary around average values of 1.8%. The natural authigenic ^{10}Be concentration measurements were performed at the French AMS national facility ASTER (CEREGE). ^{10}Be sample concentrations are calculated from the measured spiked ^{10}Be/^{9}Be ratios normalized to the BeO STD-11 in-house standard ($1.191 \pm 0.013 \times 10^{-11}$; Braucher et al., 2015), and are decay-corrected using the ^{10}Be half-life ($T_{1/2}$) of 1.387 ± 0.012 Ma (Chmeleff et al., 2010; Korschinek et al., 2010). The precision (from statistical and instrumental uncertainties) of the measured ^{10}Be/^{9}Be ratios at the AMS varies around an average value of 1.5%. The uncertainties (2σ) of the calculated Be-ratio are derived from analytical error propagation and vary around an average value of 4.9%.

3. Results and interpretations

All authigenic ^{10}Be and ^{9}Be sample concentrations in atoms per gram and Be-ratios are presented versus depth in Fig. 3 and listed in supplementary material (Table S1). The results and statistical averages are reported hereafter with a $\pm 2\sigma$ uncertainty. The authigenic ^{9}Be concentrations vary from 0.74 to 2.46×10^{16} at.g^{-1} with an average value and standard deviation of $1.70 \pm 0.25 \times 10^{16}$ at.g^{-1} (Fig. 3b). The sample #22-65 from the foraminiferal reworked sandy layer at the bottom of the studied interval (3297 cm; Fig. 2) exhibits a sharp ^{9}Be content increases ($3.06 \pm 0.07 \times 10^{16}$ at.g^{-1}). This result largely deviates from the authigenic ^{9}Be average concentration likely because of the major environmental change associated with the reworked sandy layer deposition. It induces a Be-ratio of $1.35 \pm 0.08 \times 10^{-8}$, far outside the Be-ratio range defined by all other values, i.e. 2.32 to 7.12×10^{-8}, and significantly lower than its long-term average and standard deviation: $4.68 \pm 1.01 \times 10^{-8}$ (Fig. 3d), and was therefore exclude for geomagnetic interpretation. The authigenic ^{10}Be (decay-corrected) concentrations vary from 3.60 to 15.77×10^{8} at.g^{-1} with an average value and standard deviation of $7.88 \pm 1.96 \times 10^{8}$ at.g^{-1} (Fig. 3c). The sedimentary homogeneous interval from 1470 to 2200 cm (MIS 18 to 43) yields ^{9}Be and ^{10}Be concentrations that oscillated within the $\pm 1\sigma$ range except for few peaks presenting values above the mean $+1\sigma$ limit. Amongst these peaks, the highest ^{10}Be concentrations are found between 1538–1558 cm depth and are accompanied by coincident high ^{9}Be values. This interval corresponds to the MBT. Few ^{9}Be peaks appear in intervals related to glacial stages or to interglacial–glacial transition. They can be explained by lithogenic enhancements from the nearby exposed Benham Bank during low sea level episodes. The ^{10}Be variations do not present such glacial/interglacial signature (Fig. 3c). Moreover, the normalization of ^{10}Be by the ^{9}Be does not introduce such climatic distortion and provides a Be-ratio peak series coherent with RPI minima and/or polarity shifts supporting their geomagnetic origin (Fig. 3d–f).

From 2200 cm to the bottom of the studied interval, large amplitude variations are recorded on both ^{9}Be and ^{10}Be records: ^{9}Be concentrations are high and ^{10}Be concentrations vary around the mean-1σ, leading to Be-ratio values lower than the mean-1σ. This is especially verified between 2380 and 2800 cm depth where lower magnetic susceptibility values (about 80% of the average MS; Fig. 2b) characterize the MIS 49–65 succession. The average Be-ratio decrease by ~75% is therefore likely the result of an environmental bias associated with the presence of three thick tephra layers and significant volcanic ashes dissemination from intense volcanic activity in the Macolod Corridor, southwestern part of the Luzon island (Fig. 1). This sedimentary artefact probably modified the Be inputs and/or changed mixing and scavenging rates of dissolved Be in the water column. Namely, additional ^{9}Be inputs delivered by successive eruptions and non related to normal denudation processes together with potential incomplete mixing of dissolved ^{9}Be and ^{10}Be in the water column may have favored an inadequate normalization leading to biased Be-ratios at these levels. Unfortunately, no paleomagnetic cubes have been sampled in the tephra layers precluding any identification of sharp ^{9}Be peaks in these units as observed in Simon et al. (2017). Additional results from other cores will be helpful in order to verify/estimate the potential remaining environmental imprint and eventually evaluate its importance. However, the clear identification of Be-ratio peaks in phase with RPI minima and polarity reversals in this interval, and more largely, in the whole MD97-2143 core confirms the reliable identification of ^{10}Be overproduction episodes associated with GDM collapses during the Matuyama's chron (Figs. 3 and 4), and yields for the first time a ^{10}Be-derived GDM reconstruction down to ca. 2.1 Ma.

4. Comparison between Be-ratio and RPI records

The comparison of the standardized RPI and Be-ratio records presented in Fig. 4 is consistent with a first order dependence from a common forcing: the geomagnetic dipole moment variation. The Be-ratio peaks are systematically associated with deep RPI minima with stratigraphic offsets between 2 and 14 cm (Fig. 4a–f) or ~2 to 12 ka. Since the residence time of the ^{10}Be in the water column ranges from ~100 years at Pacific Ocean margins to less than 1 ka in the western Pacific Ocean (von Blanckenburg and Igel, 1999), it may account for a maximum depth offset of ~1 cm (~1 ka). Bioturbation in the surficial mixing layer can also impact the Be-ratio by filtering its signature over a significant thickness that can be evaluated at 15–20 cm in core MD97-2143 according to the vertical redistribution of the instantaneous deposited Australasian microtektite layer (Lee and Wei, 2000). Using the same microtektite deconvolution strategy for the ^{10}Be signal of the MBT from two distinct records, Suganuma et al. (2011) and Valet et al. (2014) found no stratigraphic displacement induced by bioturbation filtering relatively to the RPI recording. The stratigraphic offsets can thus be attributed to the post-depositional magnetic grain realignments before compaction/dewatering that leads to delayed magnetization locking-in. Previous comparisons between the respective positions ^{10}Be-peaks and RPI minima have also attributed similar depth offsets ranging from 0 to 30 cm in a variety of sedimentary environments to post-depositional remanent magnetization (pDRM) (Carcaillet et al., 2003, 2004; Knudsen et al., 2008; Suganuma et al., 2010, 2011; Ménabréaz et al., 2012; Valet et al., 2014). This pDRM low-pass filter smoothes the signal and locks paleomagnetic signatures of directions and RPI in underlying sediment layers leading to an age offset (aging) of paleomagnetic signatures versus their input geomagnetic signal (Roberts and Winklhofer, 2004; Roberts et al., 2013). Because of variable physical, chemical and biological characteristics of sediments (e.g. clay or carbonates content, flocculation particles size, amount of biogenic/detrital magnetite), the attempts to model pDRM lock-in depths have been rather limited and the direct comparison of ^{10}Be and RPI series provide therefore a unique mean to estimate pDRM lock-in depths.

The higher density of the sampling across several reversals and excursions provides an adequate resolution enabling estimation of the lock-in depths at several control points. The largest

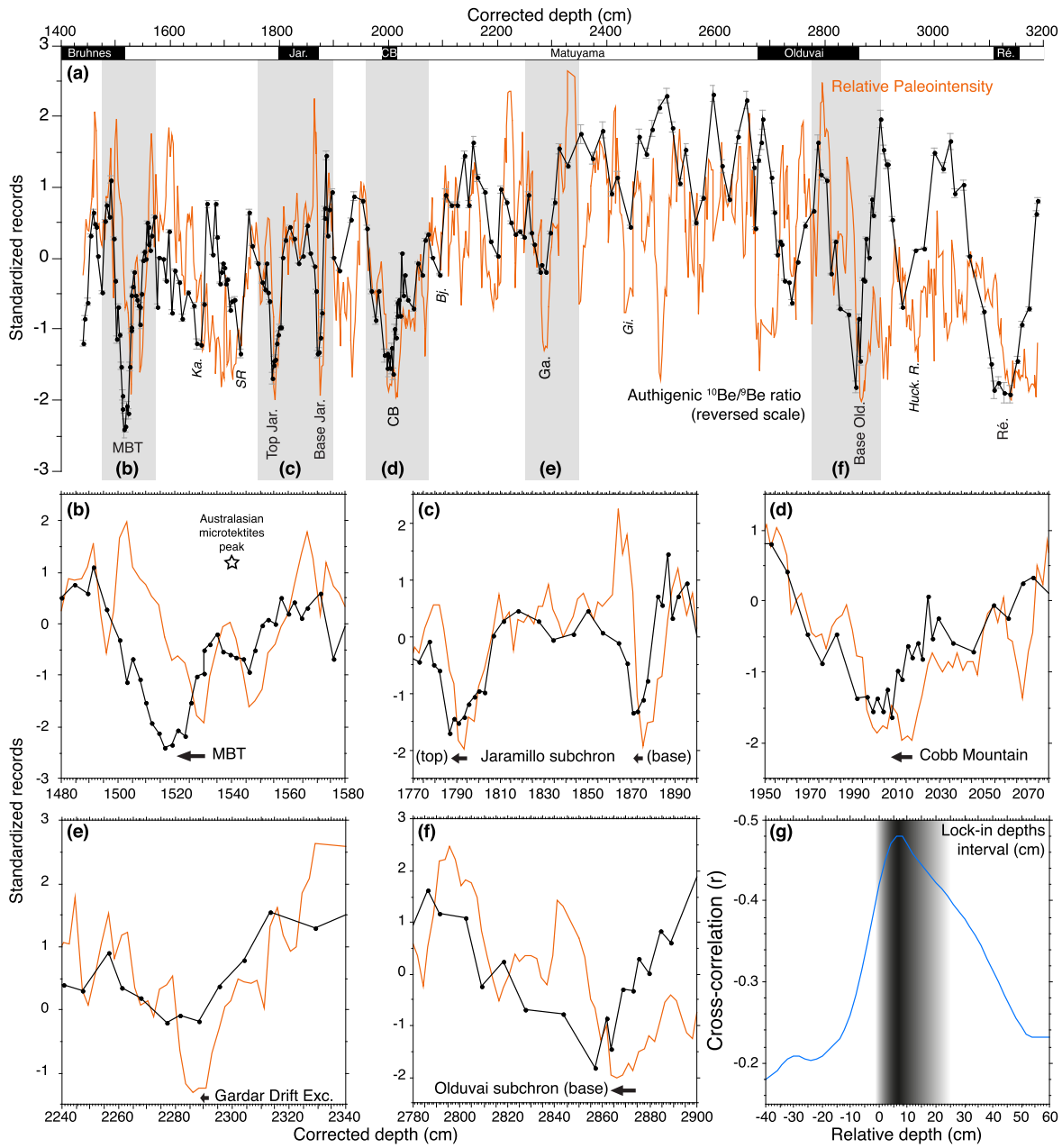

Fig. 4. Comparison between the Be-ratio and RPI records on corrected depth scale. (a) Standardized records: RPI (orange) and Be-ratio in black (note that the scale is reversed for a direct comparison with RPI). (b–f) Snapshots centered on: (b) the Matuyama–Brunhes transition (MBT), (c) Jaramillo subchron, (d) Cobb Mountain event, (e) Gardar drift excursion and (f) Olduvai subchron base. (g) Cross-correlation between the Be-ratio and RPI records. The grey area covers the range of lock-in depths with higher density values comprised between 4 and 10 cm. Geomagnetic events (reversals and excursions) have been labeled and refer to the geomagnetic polarity time scale (top): MBT (Matuyama–Brunhes transition), Ka. (Kamikatsura), SR (Santa Rosa), Jar. (Jaramillo), Pu. (Punaruu), CB (Cobb Mnt), Bj. (Bjorn Exc.), Ga. (Gardar Drift), Gi. (Gilsa), Old. (Olduvai), Huck. R. (Huckelbury Ridge), Ré. (Réunion). (For interpretation of the references to color in this figure legend, the reader is referred to the web version of this article.)

stratigraphic offset between the Be-ratio peak sequence and the paleomagnetic sequence is recorded at the MBT: the Be-ratio peak is recorded 14 cm above the minimum RPI and polarity reversal, which corresponds to ~11 ka offset toward younger ages, conformably to the results of Suganuma et al. (2010) (Fig. 5). Post-depositional locking-in processes are further suggested by the fact that minimum RPI values are associated with positive inclinations values, as if partial re-magnetization was imposed in the normal subsequent strong field. It is indeed very unlikely that inclinations could reach stable GAD values during the dipole moment low, while a re-magnetization in high field after recovery of the normal polarity dipole moment would explain the observed high (near GAD) inclination values.

Fig. 5 also shows that the Be-ratio reproduces small-scale RPI variations that are not apparent using the ^{10}Be-flux method. This observation further supports the requirement of using normalization processes in order to eliminate secondary environmental imprints prior to any reliable geomagnetic interpretations of ^{10}Be records.

Outside from the ^{10}Be overproduction episode associated with the MBT, the Be-ratio record exhibits other significant enhancements coherent with RPI variations along the core (Figs. 3 and 4). These overproduction episodes are also affected by depths offsets which are removed when the two series (RPI and Be-ratio) are shifted by 4 to 10 cm (Fig. 4g). Considering the sedimentation rates, this corresponds to time delays of 3 to 8 ka probably

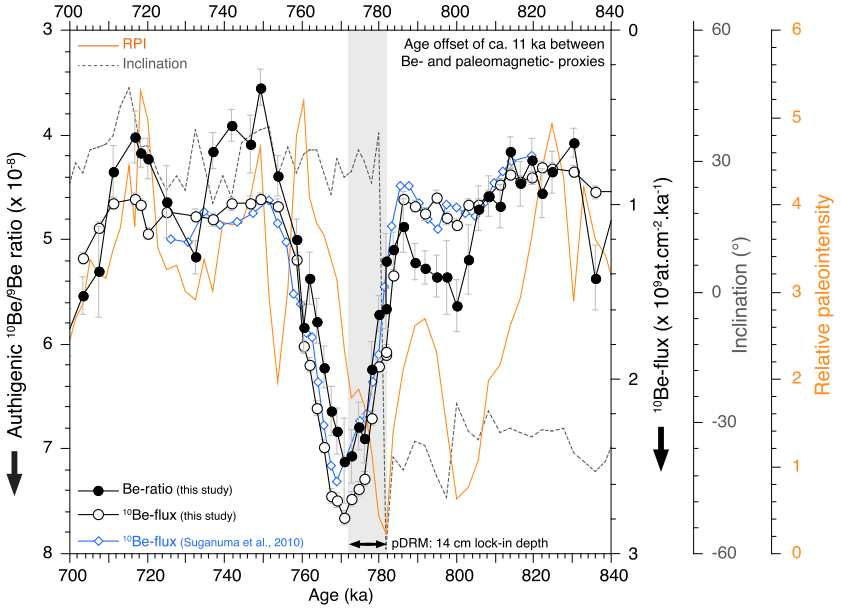

Fig. 5. Comparison of paleomagnetic results and Be-series at the Matuyama–Brunhes transition (MBT). The Be-ratio from this study (black dots) is compared to raw ^{10}Be-flux (^{10}Be concentration × bulk density × sedimentation rate) calculated on our ^{10}Be results (black empty dots) and from the Suganuma et al. (2010) study (empty blue diamonds). The RPI (orange) and inclination (grey dashed line) are from Horng et al. (2002, 2003). (For interpretation of the references to color in this figure legend, the reader is referred to the web version of this article.)

assignable to the pDRM lock-in depth function. The processes associated with pDRM could also contribute to smooth the recording of rapid directional changes in such a low sedimentation rate core, explaining the absence of directional deviation recording for most of the excursions that occurred during the studied time interval (Fig. 3f).

5. Matuyama–Brunhes transition (MBT)

Despite the fact that the MBT is by far among the most studied past geomagnetic reversal (e.g. Valet and Fournier, 2016), its accurate age is still debated. The reasons of such uncertainties are related to several factors, e.g. i) variable ^{40}Ar/^{39}Ar dating calibration applied to transitional lava flows or tephra layers, ii) multicomponent magnetization in paleomagnetic records that complicate genuine geomagnetic reading, iii) imperfect or inaccurate astrochronological calibration of sediment sequences, iv) inaccurate stratigraphic positioning of the transition due to poor understanding of magnetization acquisition processes or negligence of pDRM lock-in depth effects, mostly in low sedimentation rate sequences. For example, the MBT age was recently inferred at 783.4 ± 0.6 ka from ODP Site 758 based on a tephrochronological approach (Mark et al., 2017). However, added to the poor resolution of the paleomagnetic and δ^{18}O records, the fact that potential pDRM effects were neglected in such low sedimentation rate context (<2 cm/ka), hampers any confidence to this result, despite robust radiometric (^{40}Ar/^{39}Ar) datum. Referring to the literature, the MBT ages are divided into two distinct groups: ~770–775 ka and ~780–785 ka (e.g. Tauxe et al., 1996; Channell et al., 2010; Singer, 2014; Mark et al., 2017). Fig. 5 highlights a clear picture of the MBT from Be- and paleomagnetic-measurements in the MD97-2143 core. The 1.5-fold Be-ratio increase represents a ^{10}Be overproduction episode centered at 772 ka and spanning the 764–780 ka time interval. A corresponding long duration ^{10}Be overproduction episode was also observed in marine cores and in the EPICA Dome C (EDC) ice record that coincides with the minimum VADM values in the PISO-1500 stack at ~767–778 ka (Fig. 6b–c). The GDM collapse is synchronous with the minimum summer insolation following the maximum summer insolation that triggered the MIS 19c/20 transition (Fig. 6a–b). This allows to assign the MBT to the ~770–775 ka range which agrees with the highest resolution paleomagnetic records from North Atlantic IODP sites (Channell et al., 2010). It is further supported by reliable radiometric dating from the transitional Haleakala lava flow (772.0 ± 2.0 ka; Singer et al., 2017), Montalbano Jonico section (773.9 ± 1.3 ka; Petrosino et al., 2015; Simon et al., 2017) and Chiba record (770.9 ± 7.3 ka; Suganuma et al., 2015; Okada et al., 2017).

Prior to the MBT, marked intensity lows are frequently reported from both marine sediments and lava flows records suggesting the occurrence of a precursor event before the reversal (Hartl and Tauxe, 1996). A ^{10}Be flux peak in the EDC record (Fig. 6b) may be considered as another clue but failed to be recorded in most other available marine records (Fig. 6b). The present MD97-2143 record does not evidence any indisputable ^{10}Be overproduction episode before the MBT but is rather characterized by a plateau after an initial increase between 795–805 ka. The only notable exception is observed in core MD98-2187 where a long duration (~30 ka) ^{10}Be-flux peak is recorded over the whole pre-MBT/MBT time interval (Suganuma et al., 2010). Since the ^{10}Be variation is not normalized for secondary environmental imprints using the ^{10}Be-flux approach, one can question the pristine geomagnetic origin of this long duration ^{10}Be increase interval, especially within the deglacial transition between MIS 19c/20 (Termination I.X). Altogether, the absence of a clear ^{10}Be overproduction episode prior to the MBT in most records, including Chinese loess (Zhou et al., 2014), raises questions, especially since all GDL associated with excursions during the Brunhes chron are confirmed by significant ^{10}Be overproduction episodes (e.g. Simon et al., 2016a). Whether this peculiar ^{10}Be signature results from low sampling resolution, environmental imprint or reveals geodynamo processes remains unclear.

6. Mid to late Matuyama chron GDM instabilities inventory

Among reversals, geomagnetic events and excursions documented in marine sediments and lava flows during the mid to late Matuyama chron (ca. 772–2140 ka), the boundaries of the Jaramillo and Olduvai subchrons constitute robust magnetostratigraphic markers. By contrast the Cobb Mountain and Réunion

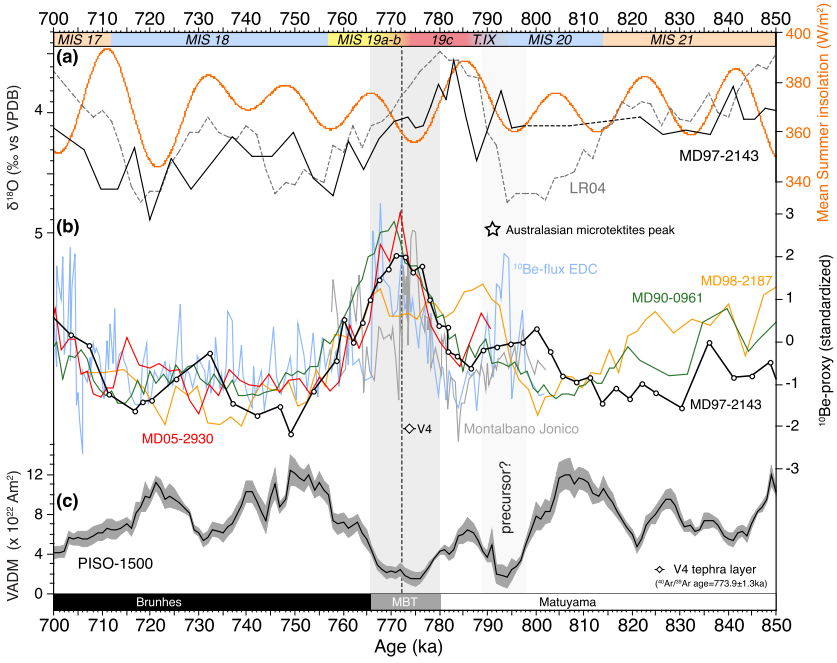

Fig. 6. Geomagnetic dipole moment signature of the MBT from cosmogenic radionuclide ^{10}Be and RPI records. (a) Oxygen isotope stratigraphy from core MD97-2143 and LR04 stack (grey dashed line) from Lisiecki and Raymo (2005). Mean summer insolation at 65°N is from Laskar et al. (2004). (b) Standardized Be-ratios from cores: MD97-2143 (this study), MD05-2930 (Ménabréaz et al., 2014; Simon et al., 2016a), MD90-0961 (Valet et al., 2014) and Montalbano Jonico (Simon et al., 2017). The Montalbano Jonico Be-ratio series is placed on the new chronology (Nomade et al., in prep.). The ^{40}Ar/^{39}Ar age of the V4 tephra layer lying within the Be-ratio peak in the Montalbano Jonico succession is 773.9 ± 1.3 ka (Petrosino et al., 2015). Standardized ^{10}Be-flux from EDC (Raisbeck et al., 2006) and from core MD98-2187 (Suganuma et al., 2010). (c) PISO-1500 stack (Channell et al., 2009).

events are often recorded as long duration RPI lows occasionally accompanied by transient polarity instabilities (Fig. 3e–f). Few excursions are also reported in the late Matuyama epoch (e.g. Singer, 2014; Laj and Channell, 2015; Channell, 2017). The following discussion compares our original ^{10}Be-inventory with paleomagnetic references (Table 1). The ages of the GDM instabilities leading to significant ^{10}Be overproduction episodes are inferred from the mid Be-ratio peaks, while their durations are estimated from the peaks width between inflexion points (not taking into account limitations due to sampling resolution and age uncertainties). Other long-term Be-ratio records have been used for comparison, but two of them cover the MBT and late Matuyama interval only. Core MD97-2140 (Carcaillet et al., 2003) placed on the benthic δ^{18}O chronology of de Garidel-Thoron et al. (2005) has been also used for comparison, though it only goes down to ~1300 ka (Fig. 7c). Despite its low sampling resolution and high uncertainties, this record complements results of core MD97-2143 and further support geomagnetic interpretations in the 800 to 1300 ka time interval.

Together with the available radiometric ages, the GDL time series was established using the first principal component (PC1) compute from the PISO-1500, SINT-2000 and PADM2M stacks, and with IODP Site U1308 for older events (>2 Ma). The aim of using a principal component analysis here is not to provide with a new RPI index, but to extract an inventory of the largest dipole lows from these references. PC1 explains most of the variance and yields a series of GDL coherent with the Be-ratio peaks (Table 1 and Figs. 7g and 8g). Despite some redundancy due to the fact that stacks contain many of the same records, PC1 illustrates the geomagnetic dipole moment variability characterized by recurrent collapses correlated with ^{10}Be overproduction episodes. The largest chronological mismatches between the MD97-2143 Be-ratio record and PC1 are 12 ka (Santa Rosa, 942 ka), 22 ka (Punaruu, 1101 ka) and 32 ka (unnamed event at 1380 ka), and 20 ka (Réunion top, 2096 ka) with IODP Site U1308 (Channell et al., 2016). Excluding these four events, the average age offset computed for the rest of the GDL population is 5 ± 5 ka (Table 1), representing a mean 0.4% lag.

The brief description of Be-ratio peaks associated with reversals, geomagnetic events or excursions are divided in two subsections and figures, i.e. 800–1300 ka and 1300–2140 ka, based on sedimentological interpretations (see section 3) and available complementary Be-ratio records. The sediment homogeneity as well as the compilation of Be-ratio records allows robust geomagnetic interpretations between 800 and 1300 ka (Fig. 7). Possible biases of the Be-ratio due to thick tephra layers and their vertical dissemination introduce uncertainties in the 1300–2140 ka interval (Fig. 8), despite the fact that Be-ratio peaks recorded in phase with RPI minima and polarity reversals in the whole MD97-2143 core supports the efficiency of the ^{9}Be normalization (Figs. 3–8).

6.1. GDL in the 800–1300 ka time interval

This interval is marked by five clearly identified ^{10}Be overproduction episodes presenting 1.3- to 1.4-fold Be-ratio increases compared to the Be-ratio average (Fig. 7c). These episodes are accompanied by RPI minima in core MD97-2143 and references (Fig. 7d–f). Directional transitions associated with the Jaramillo subchron boundaries and the Cobb Mountain event also characterized three of these episodes (Fig. 7b). A short normal polarity is attributed to the Santa Rosa excursion in core MD97-2143 (920–924 ka) but the associated RPI signal (two distinct lows at 916 and 932 ka) does not correspond to the well-defined VADM low (930 ka) followed by higher values from the PISO-1500 and SINT-2000 stacks, which are consistent with the Be-ratio despite a slight age offset of 12 ka. This observation likely implies a problem in the original RPI record and leaves with an unsolved chronological issue for this event.

Chronologically, these major ^{10}Be overproduction episodes can be tied to the following geomagnetic events (ages between brackets correspond to the mid Be-ratio peaks): Kamikatsura (884 ka; MIS 22), Santa Rosa (942 ka; MIS 24–25), Jaramillo top (991 ka;

Table 1
Mid- to late Matuyama chron geomagnetic dipole lows (GDL) associated with polarity reversal and excursions.

Label[a]	This study		Horng et al. (2002)[c]		Channell et al.[d]		Singer (2014)[f]		GPTS[g]	ICS Global	Hag2017[i]	Corresponding
	MIS	Age ± uncertainty (ka)[b]	MIS	Age (ka)	MIS	Age (ka)	$^{40}Ar/^{39}Ar$ ages	GITS (ka)	(ka)	v.2016a[h]	$^{40}Ar/^{39}Ar$ ages	GDL[j]
Matuyama–Brunhes transition (MBT)	19a–b	772 ± 8	19	781	19	773	772 ± 2	773	781	774	778 ± 4	775
Precursor	20	800 ± 2?					793	794				794
Kamikatsura	22	884 ± 4			22/23	888	900 ± 5	906		885	886 ± 3	888
Santa Rosa	24–25	942 ± 4	23–24	916/932	25	932	932	932		932		930
Jaramillo top	28a	991 ± 9	27	988	27	990	1001	1008	988	990	972 ± 3	990
Intra-Jaramillo?	*30*	*1045 ± 3*[*]			30/31	1051	1048	1048				1044
Jaramillo base	31	1071 ± 4	31	1072	31	1071	1069	1076	1072	1071	1072 ± 5	1071
Punaruu?	32	1101 ± 7[*]			32–34	1115 (1092–1122)	1122	1129		1123	1105 ± 5	1123
post-Cobb Mnt.?	*35*	*1161 ± 5*[*]										1155
Cobb Mnt.	35–36	1176 / 1204 ± 5[e] (1190)	35–36	1173/1185	35/37	1190/1215	1189/1221	1189/1221	1173/1185	1187/1208	<1217 ± 4	1184–1210
Bjorn?	39	1268 ± 7[*]			38	1251–1255		1255		1255		1275
Unnamed	44–45	1380 ± 7										1348
Gardar	48	1459 ± 9			49	1455–1476		1472–1480		1475		1463
Gilsa	54–55	1587 ± 8			54	1551–1584		1567–1575		1584		158-2-1584
Unnamed	59	1687 ± 9										1686
Olduvai Top	63	1770 ± 4	63–64	1778	63	1778–1780	1775	1787	1778	1780		1778–1782
Unnamed	66–67	1839 ± 17										
Olduvai Base	71	1934 ± 8	71–72	1945	(71) 73	1945 (1925)	1922	1934	1945	1925	1976 ± 10–1965 ± 12	1925–1931
Huckelbury Ridge	76	2004 ± 8					2070	2070				2000
Réunion (or Feni?)	79–80	2096/2124 ± 5 (2110)	80–81	2118/2133	80/81	2115–2153	2115/2153	2120/2155	2128/2148	2116/2137		2116/2137

[a] Labels are used for easy geomagnetic events identification and are reviewed in Singer (2014) and Laj and Channell (2015). Names in bold represent polarity reversals. Names in italics and marked with a question mark are assumed given their chronology with references but are not significant in our record and deserve later confirmations.

[b] Ages are based on the identification of the Be-ratio mid-peaks. The uncertainty are computed from the Be-ratio peaks width (between inflexion points) and correspond to the duration of the GDL.

[c] Ages are based on the identification of RPI lows in the MD97-2143 core according to the Horng et al. (2002) age model. The revised chronology places the Cobb Mnt (RPI low) at 1092/1205 ka.

[d] Channell et al. (2002, 2009, 2016) and Channell (2017). See text for details.

[e] Ages of the top/base boundaries of geomagnetic events.

[f] Reviewed ages proposed from several Singer et al. papers (1999–2013). Age of the MBT is from new measurements on the Haleakala lava (Maui) by Singer et al. (2017; GSA Paper No. 352-4).

[g] Lourens (2004); Ogg (2012).

[h] Cohen and Gibbard (2016).

[i] Hagstrum et al. (2017).

[j] Ages in the 700–1500 ka interval are from the PC1 of the PCA analysis on PISO-1500 (Channell et al., 2009), SINT-2000 (Valet et al., 2005) and PADM2M (Ziegler et al., 2011) RPI stacks. Ages in the 1500–2140 ka interval are from IODP U1308 (Channell et al., 2016) (Fig. 8).

[*] Ages inferred from the Be-ratio records from cores MD97-2143 and MD97-2140 (Carcaillet et al., 2003).

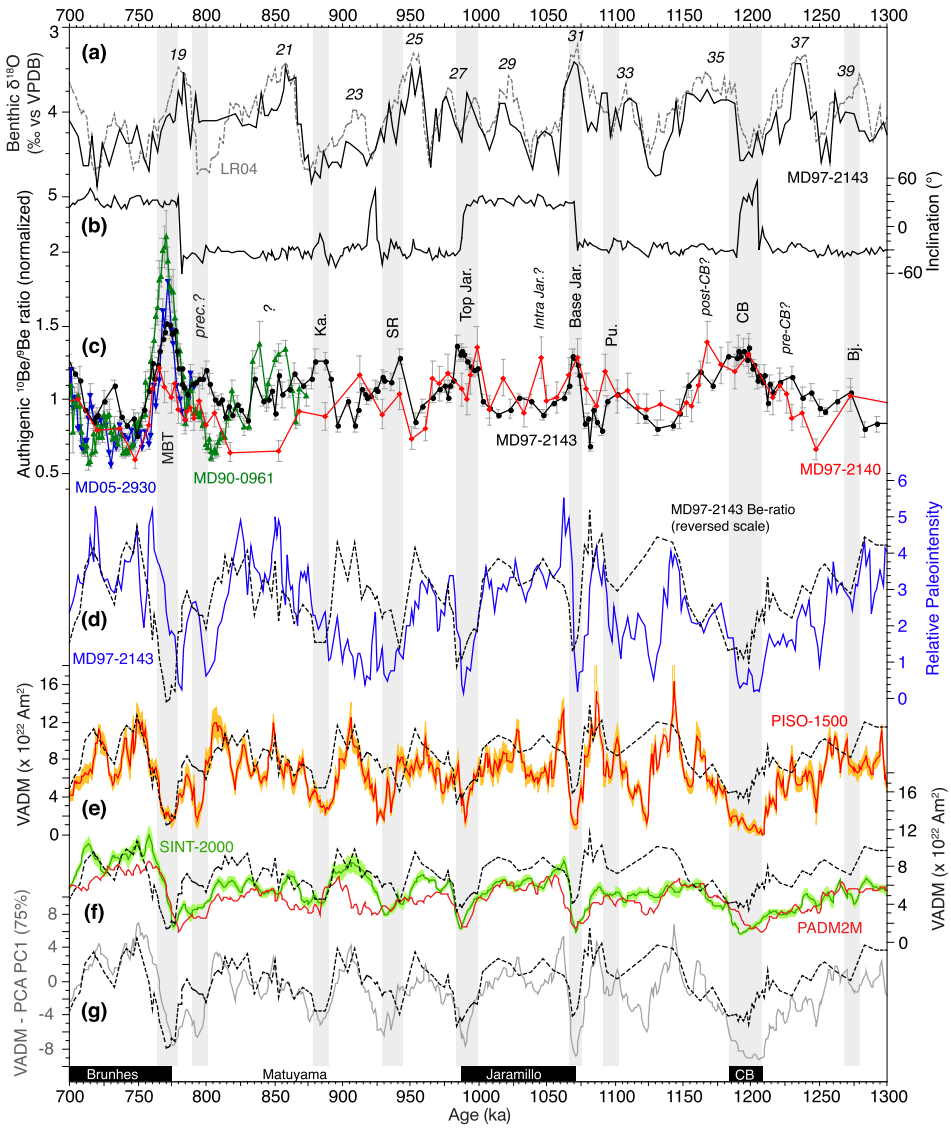

Fig. 7. Geomagnetic field changes in the 700–1300 ka time interval. (a) Benthic $\delta^{18}O$ record in black compared to the LR04 stack in grey. (b) MD97-2143 inclination. (c) Normalized Be-ratios of MD97-2143 (black), MD05-2930 (blue; Ménabréaz et al., 2014), MD90-0961 (green; Valet et al., 2014), MD97-2140 (red; Carcaillet et al., 2003). (d) MD97-2143 RPI record. (e–f) RPI stacks: (e) PISO-1500 (Channell et al., 2009), (f) SINT-2000 (green, Valet et al., 2005) and PADM2M (red, Ziegler et al., 2011). (g) The first principal component extracts by PCA analysis on the PISO-1500, SINT-2000 and PADM2M records (grey curve) explains 75% of the variance and yields a series of GDL in phase with ^{10}Be overproduction episodes. (d–g) The MD97-2143 Be-ratio (black dashed line) is plotted on a reversed scale. Geomagnetic events (reversals and excursions) have been labeled and refer to the geomagnetic polarity time scale (bottom): MBT (Matuyama–Brunhes transition), Ka. (Kamikatsura), SR (Santa Rosa), Jar. (Jaramillo), Pu. (Punaruu), CB (Cobb Mnt), Bj. (Bjorn Exc.). (For interpretation of the references to color in this figure legend, the reader is referred to the web version of this article.)

MIS 28a), Jaramillo base (1071 ka; MIS 31) and Cobb Mountain (1190 ka; MIS 35–36) (Table 1).

The age of the Be-ratio peak associated with the Kamikatsura excursion corresponds to an excursion identified at IODP Site U1304 (Xuan et al., 2016) and U1305 (Mazaud et al., 2012) in the North Atlantic, and in lava flows from Maui (Coe et al., 2004). Immediately following this excursion, two Be-ratio peaks in core MD90-0961 and a plateau values in core MD97-2143, at ~850 ka, are not related to a reported excursion, but correspond to an interval of anomaly low VGP latitudes at ODP Site 983 (Channell et al., 2002). The Be-ratio peak corresponding to the Santa Rosa excursion takes place at the transition between MIS 24/25, as at ODP Site 983 (Channell et al., 2002) and slightly older than radiometric age of transitional directions reported in lava flows at ~926 ka (Balbas et al., 2016) and ~932 ka (Singer, 2014). Two Be-ratio peaks framing the Jaramillo subchron are coeval with GDL and polarity transitions at many sites (Table 1 and references therein). The Be-ratio peak at the Jaramillo subchron upper limit is notably synchronous with the intensity low interval measured on the transitional lava sequence from Canary Islands and dated at 996 ± 7 ka (Kissel et al., 2014). The Be-ratio peak associated with the Cobb Mountain has a long duration (~28 ka) extending over the MIS 35–36 transition and present a complex geometry with a pre- (1226 ka; MIS 37) and post- (1161 ka; MIS 35) minor ^{10}Be overproduction episodes (Fig. 7c). It coincides with a well recognized RPI low reported from both sediments and lava flows at the MIS 35/36 transition (Laj and Channell, 2015). The corresponding normal polarity in core MD97-2143 stands for ~15 ka between 1190–1205 ka, when using the adjusted chronology (see section 2.2), which is about half the duration of the associated GDL.

Along with these major episodes, three minor Be-ratio peaks are coherent with RPI minima and excursional signatures: Intra-Jaramillo (1045 ka; MIS 30), Punaruu (1101 ka; MIS 32) and Bjorn (1268 ka; MIS 39). The intra-Jaramillo GDL is suggested by a single Be-ratio outlier in core MD97-2140 (Carcaillet et al., 2003),

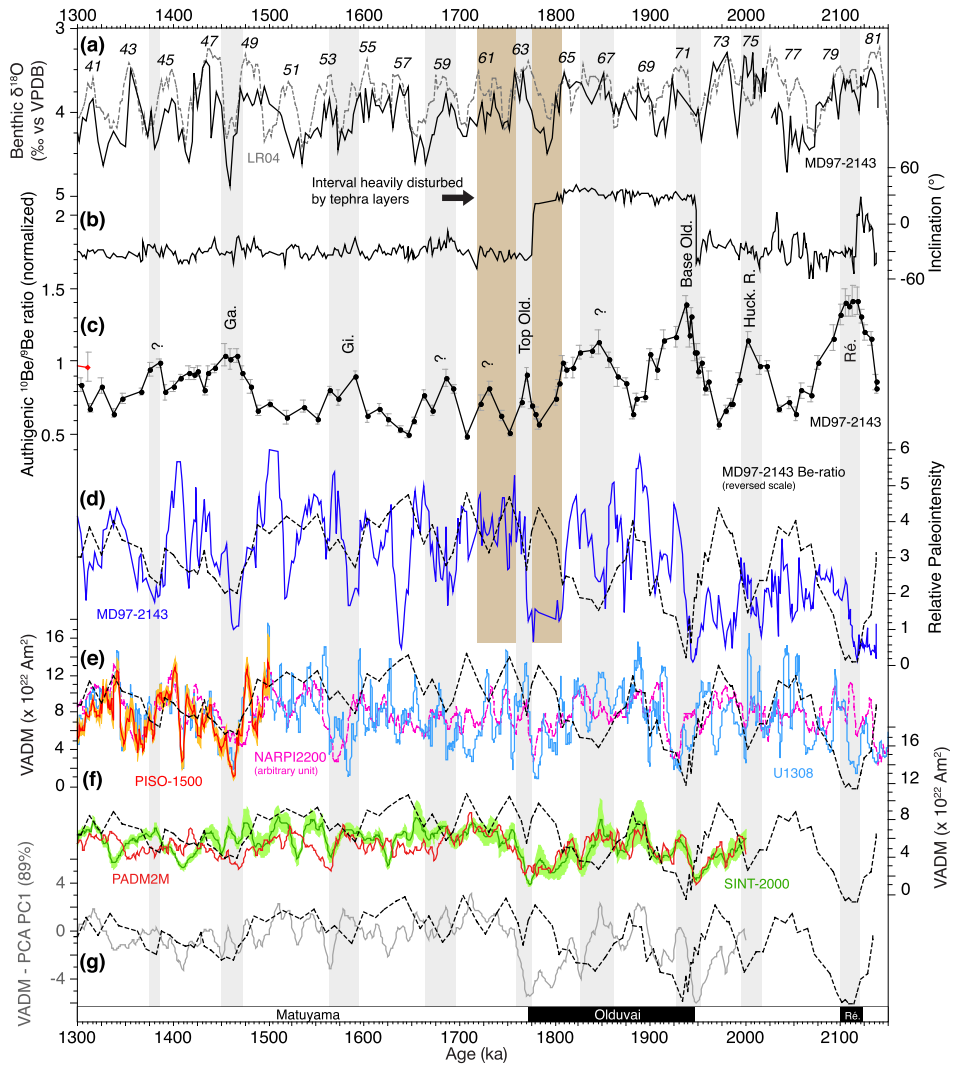

Fig. 8. Geomagnetic field changes in the 1300–2140 ka time interval. (a) Benthic $\delta^{18}O$ record in black compared to the LR04 stack in grey. (b) MD97-2143 inclination. (c) Normalized Be-ratios records of MD97-2143. (d–f) RPI records: (d) MD97-2143, (e) PISO-1500 stack (Channell et al., 2009), IODP U1308 site and NARPI-2200 stack (Channell et al., 2016), (f) SINT-2000 (Valet et al., 2005) and PADM2M (Ziegler et al., 2011). (g) The first principal component extracts by PCA analysis on the SINT-2000 and PADM2M records (grey curve) explains 89% of the variance yielding a series of GDL in phase with ^{10}Be overproduction episodes. (d–g) The MD97-2143 Be-ratio (black dashed line) is plotted on a reversed scale. Geomagnetic events (reversals and excursions) have been labeled and refer to the geomagnetic polarity time scale (bottom): Ga. (Gardar Drift Exc.), Gi. (Gilsa Exc.), Huck. R. (Huckelbury Ridge), Ré. (Réunion).

which appears at the same time interval than excursional directions recorded at North Atlantic ODP Sites 983, 984 and U1306 (Channell et al., 2002). A Be-ratio outlier recorded at 1101 ka (MIS 32) is also consistent with excursional directions reported both from the Punaruu lavas in Tahiti (Singer et al., 1999) and from North Atlantic (Xuan et al., 2016; Channell, 2017) and California margin (Guyodo et al., 1999) sedimentary sequences. Another Be-ratio signal coherent with a RPI minimum can be inferred during the MIS 39 interval (1268 ka) and is tentatively associated to the Bjorn excursion which has been recognized in records from the North Atlantic (Channell, 2017). Indisputable identification of these events requires further validations, but the temporal relationship between Pacific and North Atlantic records suggest a global signature of these excursions.

6.2. GDL in the 1300–2140 ka time interval

This interval is marked by ten identified intervals evidencing 1.6- to 2.4-fold Be-ratio increases compared to their framing interval (Fig. 8c). The drop of the long-term Be-ratio average, likely related to environmental bias, hampers any quantitative estimation of their real amplitudes, and request complimentary Be-ratio records to interpret their signatures. However, the synchronicity of these Be-ratio peaks with RPI minima in core MD97-2143 and other reference records (Fig. 8d–f), as well as polarity reversals of the Olduvai subchron boundaries confirm their geomagnetic significance (Fig. 8b). Based on their chronology, these events are assigned to the Gardar excursion (1459 ka; MIS 48), Gilsa excursion (1587 ka; MIS 54–55), Olduvai subchron boundaries (1770/1934 ka MIS 63 / 71), Huckelbury Ridge excursion (2004 ka; MIS 76) and the Réunion event (2096/2124 ka; MIS 79–80). Three other Be-ratio peaks at 1380 ka (MIS 44–45), 1687 ka (MIS 59) and 1839 ka (MIS 66–67) correspond to RPI minima but are not associated to recognized excursions (Table 1).

The Be-ratio peaks documenting the Gardar and Gilsa GDL match with transitional direction and RPI minima from high-resolution cores from the North Atlantic (Xuan et al., 2016; Channell, 2017 and references therein). The large Be-ratio peak at the base of the Olduvai is coeval with RPI minima (Fig. 8d–g) and with the GITS chronology (Singer, 2014). A small Be-ratio peak dated at 1770 ka (MIS 63) is coherent with the upper boundary of the Olduvai subchron but its expression is probably largely af-

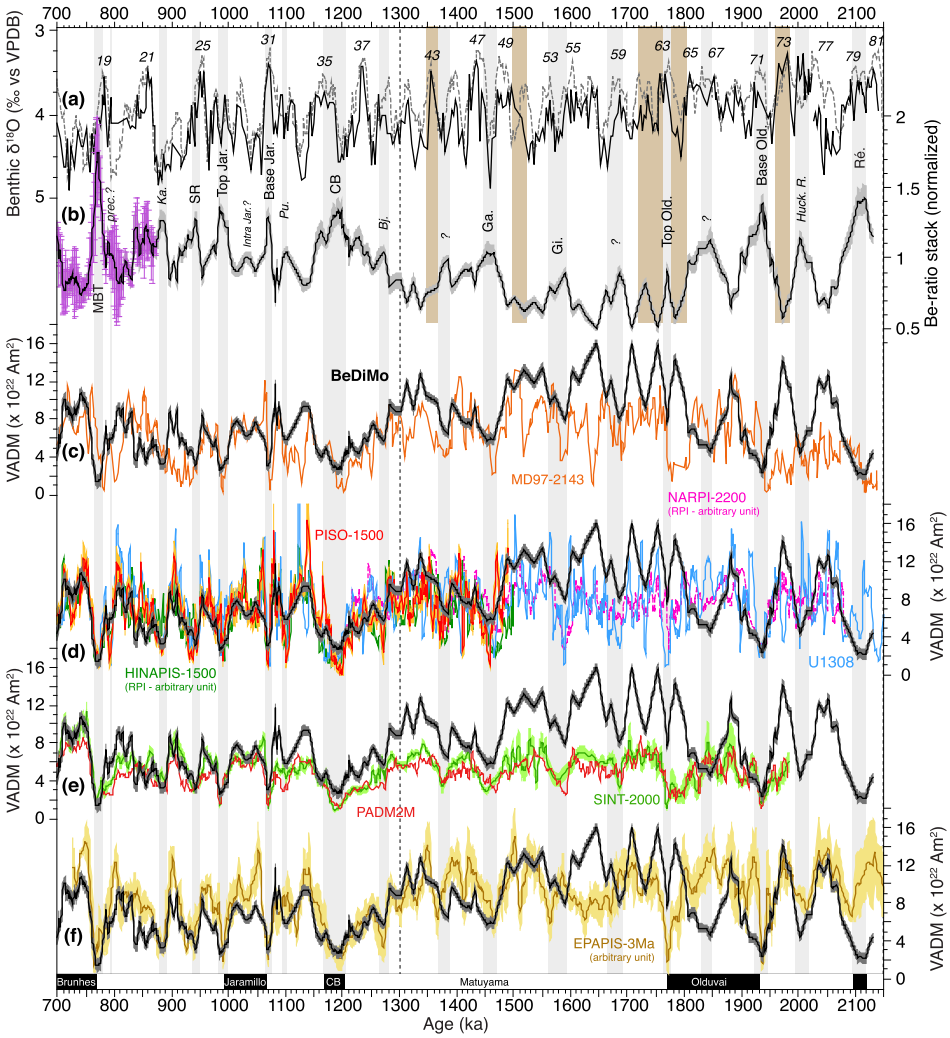

Fig. 9. Be-ratio compilation and ^{10}Be-derived Dipole Moment record over the 700–2140 ka time interval (BeDiMo) compare to references. (a) Benthic δ^{18}O record of core MD97-2143 in black compared to the LR04 stack in dashed grey. (b) Normalized Be-ratios composite record (see text). (c–f) The BeDiMo (black curve) is compared to: (c) the MD97-2143 VADM-derived curve (orange) using the PADM2M model for scaling (Ziegler et al., 2011), (d) PISO-1500 stack (red; Channell et al., 2009), HINAPIS-1500 stack (green; Xuan et al., 2016), NARPI2200 stack (pink) and IODP Site U1308 (blue) (Channell et al., 2016), (e) the SINT-2000 stack (green; Valet et al., 2005) and PADM2M model (red, Ziegler et al., 2011) and (f) the EPAPIS-3M stack (Yamazaki and Oda, 2005). All individual chronologies have been aligned on the BeDiMo age scale. The absolute BeDiMo values older than 1300 ka are likely overestimated given potentially bias on the Be-ratio resulting from environmental imprints (see text). Geomagnetic events (reversals and excursions) have been labeled and refer to the geomagnetic polarity time scale (bottom): MBT (Matuyama–Brunhes transition), Ka. (Kamikatsura), SR (Santa Rosa), Jar. (Jaramillo), Pu. (Punaruu), CB (Cobb Mnt), Bj. (Bjorn Exc.), Ga. (Gardar Drift Exc.), Gi. (Gilsa Exc.), Old. (Olduvai), Huck. R. (Huckelbury Ridge), Ré. (Réunion). (For interpretation of the references to color in this figure legend, the reader is referred to the web version of this article.)

fected by the stratigraphic vicinity with two thick tephra layers (Fig. 8). The large Be-ratio peak at 2004 ka (MIS 76) may be related with the Huckelbery Ridge excursion also reported from ODP Site 981 (Channell et al., 2003), but its dating does not agree with the recent ^{40}Ar/^{39}Ar age of 2070 ka obtained from the Huckleberry Ridge Tuff (Singer, 2014). The large Be-ratio peak centered at ~2110 ka (2096–2124 ka; MIS 79–80) can be assigned to the Réunion event dated in the same time interval (Roger et al. 2000; Channell et al., 2003; Singer, 2014).

7. Be-geomagnetic dipole moment

The calibration method introduced by Carcaillet et al. (2004) and further improved by Simon et al. (2016a) allowed to reconstruct a ^{10}Be-derived GDM record using normalized Be-ratio record and absolute virtual (or virtual axial) Dipole Moment values (i.e. VDM or VADM) extracted from the Geomagia50.v3 (Brown et al., 2015) and PINT2015-05 databases (http://earth.liv.ac.uk/pint/; Biggin et al., 2009). Reliability criteria were applied in order to extend the absolute paleointensity dataset available to 2140 ka (see Supplementary Material (Fig. S2) for additional information). A Be-ratio composite record was constructed using results from cores MD97-2143 (this study), MD05-2930 (Ménabréaz et al., 2014; Simon et al., 2016a) and MD90-0961 (Valet et al., 2014) (Fig. 9b). Each normalized records has been evenly spaced and averaged by computing arithmetical means over 1 ka time windows. Uncertainties correspond to standard deviations computed between overlapping series and to the analytical uncertainties associated with the MD97-2143 core for the main part of the composite record (Fig. 9b). The uncertainties from the MIS 43–73 time interval are probably underestimated because of the environmental bias discussed in section 3. The Be-ratios from core MD97-2140 have larger uncertainties and low resolution and were not included in the stacking process. The correspondence of Be-ratio peaks with GDL supports our calibration test, especially in the sedimentary homogeneous interval (see Figs. 7 and 8). Furthermore, the empirical calibration curve obtained by polynomial regression corresponds, within the uncertainty, to the one used by Simon et al. (2016a) and to the theoretical relationship established by Masarik and Beer (2009) (see Figs. S2 and S3 in Supplementary Material

for details). The total uncertainty of the ^{10}Be-derived GDM record corresponds to the quadratic propagation of the set of errors.

The obtained ^{10}Be-derived Dipole Moment record, here entitled BeDiMo, is compared to RPI records and stacks in Fig. 9. These stacks yield a signature of the geomagnetic dipole changes, notably providing a chronological series of GDL. Their age models rely on chronological references (targets) on which all cores are synchronized (e.g. IODP U1308 for the PISO-1500; ODP Site 851 for SINT-2000; ODP Site 1143 and LR04 for EPAPIS-3M; adjusted to GPTS time scale for PADM2M). The backbones of such chronological targets are mostly based on the correlation between benthic δ^{18}O records, but these can be affected by regional offsets and depend upon sampling/data resolution and methods applied (e.g. direct or derived chronology for selected cores). Moreover, the unknown pDRM lock-in depths increase the temporal uncertainty (see section 4). Altogether, these factors cause temporal offsets reducing the accuracy of serial correlations (Table S2). In order to diminish these chronological mismatches and discuss the reliability of our new BeDiMo record, we correlated all RPI records with the BeDiMo using the main geomagnetic events and transferred them on the BeDiMo chronology (see Fig. S4 in Supplementary Material). Significant improvements are observed, especially in the most reliable time interval, i.e. 700–1300 ka, providing strong confidence on their relative variation chronology (Fig. 9; Table S2) and pinpointing GDL (Table 1; Figs. 7–9). Our new GDL inventory, independent from paleomagnetic measurements, allows to overcome the pDRM lock-in offsets induced below the mixing layer. This permits to improve time series analysis by placing the geomagnetic (^{10}Be-derived) and oxygen isotope records on a common timescale, which is vital to evaluate precisely the geodynamo rhythms and improve the knowledge of past geodynamo regimes. Our study constitutes an important first step when comparing paleomagnetic and cosmogenic studies with absolute radiometric datum (i.e. lava flows, tephra layers) but request additional higher-resolution data prior to any robust spectral analyses.

The BeDiMo average VADM reconstructed for the mid to late Matuyama chron (i.e. 772–2140 ka) – $8.0 \pm 3.2 \times 10^{22}$ Am^2 – is higher than the mean values calibrated from RPI stacks, but similar to the ones reconstructed during the Brunhes chron from the same Be-ratio approach ($7.4 \pm 2.6 \times 10^{22}$ Am^2; Simon et al., 2016a) or by RPI stacking and calibrating (see Table S3). Whether the average geomagnetic field intensity triggers, or is triggered, by the occurrence of geomagnetic events (i.e. GDM collapses) is an essential clue for understanding the geodynamo behavior (Olson et al., 2010). For example, an observation was made for the Brunhes chron about the relation between the frequency of GDL associated with excursions and the average VADM value during specific time intervals: high (low) frequencies are associated with low (high) average VADM periods (Simon et al., 2016a). A straightforward analysis of the SINT-2000 and PADM2M stacks evidences that the Matuyama chron is characterized by a high number of reversals and a low average VADM, while the stable polarity of the Brunhes chron is accompanied by a high average VADM. Our results during the late Matuyama (i.e. 772–1300 ka) permit to compute robust calibration values with an average VADM of $6.0 \pm 1.9 \times 10^{22}$ Am^2 which is statistically indistinguishable with those reconstructed from marine RPI stacks (Table S3, Fig. 9d–e). The occurrence of three successive reversals (MBT, Jaramillo boundaries) and at least 5 major geomagnetic events (including the long duration and very low intensities Cobb Mountain) during this interval of average low dipole strength supports therefore a direct relationship between both the dipole strength and its overall stability.

The BeDiMo average in the 1300–2000 ka time interval – $9.7 \pm 3.2 \times 10^{22}$ Am^2 – is significantly higher than the averages computed in the SINT-2000 and PADM2M stacks, i.e., $5.5 \pm 1.5 \times 10^{22}$ Am^2 and $5.1 \pm 1.3 \times 10^{22}$ Am^2, respectively. It is also slightly higher, but not statistically different, with values observed in the PISO-1500 stack (however limited to 1500 ka) and at site IODP U1308 site (Channell et al., 2016), $7.5 \pm 2.6 \times 10^{22}$ Am^2 and $7.8 \pm 2.9 \times 10^{22}$ Am^2, respectively (Table S3, Fig. 9d–e). This discrepancy likely results from two causes: an environmental bias affecting the Be-ratio for this time interval in core MD97-2143 (see section 3), and/or a smoothing of the RPI signal in low sedimentation rates records which constitute the SINT-2000 and PADM2M stacks. The environmental bias makes our VADM calibration highly questionable below 1300 ka, precluding any robust geomagnetic interpretation until additional data is available. The large scattered distribution of the absolute paleointensity data (Fig. S3) together with the incomplete geomagnetic events inventory during that time interval are hardly helpful to decide either. However, verifying if geomagnetic instabilities bundles arise during periods of weak geodynamo is critical for understanding the physical processes that engender geomagnetic field reversals and excursions. New integrated paleomagnetic and ^{10}Be datasets are therefore requested in order to untangle this issue and diminish uncertainties of long-term average geomagnetic field reconstruction. They will permit accurate paleointensity reconstructions, vital to confront dynamo simulations and understand the rhythms of geodynamo regimes (e.g. Thouveny et al., 2008).

8. Conclusion

The first authigenic ^{10}Be/^{9}Be ratio (Be-ratio) record spanning the 0.7–2.14 Ma time interval has been constructed from marine sedimentary core MD97-2143 (western Pacific Ocean). The Be-ratio series mirrors the RPI record with variable stratigraphic offsets: Be-ratio peaks occur 2 to 14 cm above the corresponding RPI minima, which correspond to (post-) detrital remanent magnetization (pDRM) locking-in delays of about 2 to 12 ka. The agreement between ^{10}Be overproduction episodes and the relative paleointensity (RPI) stacks SINT-2000, PISO-1500 and PADM2M supports the geomagnetic origin and confirm the global extension of the geomagnetic dipole lows (GDL). The BeDiMo (^{10}Be-derived Dipole Moment) record provides a useful complement to paleomagnetic studies permitting 1) to avoid the problem of pDRM lock-in offsets induced below the mixing layer, 2) to confront and increase the robustness and precision of GDM reconstructions and, 3) to allow future time series analysis of the geomagnetic field variations on this time interval. This study provides a critical inventory – independent of paleomagnetic methods – of major GDL linked to the Matuyama–Brunhes, Jaramillo and Olduvai polarity reversals and to short events (Cobb Mountain, Réunion). It also highlights minor GDL linked to some excursions such as Kamikatsura, Santa Rosa, Punaruu, Bjorn, Gilsa and Gardar. The long-term variations of the geomagnetic dipole field both in stable polarity state and in transitional (reversal or excursional) states are also legible. This study provides further encouragement to associate paleomagnetic and cosmogenic radionuclide beryllium-10 (^{10}Be) measurements, in order to solve pending questions about geomagnetic field instabilities and geodynamo regimes at the millennial to million-year scale.

Acknowledgements

We want to acknowledge colleagues from CEREGE: Luc Beaufort and Thibault de Garidel-Thoron for providing (chrono)stratigraphic details about cores MD97-2143 and MD97-2140, Lionel Siame for contributing to the contact between CEREGE and Academia Sinica, and Georges Aumaître and Karim Keddadouche for AMS measurements. Acknowledgments are due to Yusuke Suganuma (NIPR) for sharing the ^{10}Be data of core MD98-2187, James E.T. Channell (University of Florida) and Toshi Yamazaki (University of Tokyo) for

providing the U1308 VADM and EPAPIS-3M records, respectively. We also want to thank two anonymous reviewers for very constructive and helpful comments. The ASTER AMS national facility (CEREGE, Aix en Provence) is supported by the INSU/CNRS, the ANR through the "Projets thématiques d'excellence" program for the "Equipements d'excellence" ASTER-CEREGE action and IRD. This study is supported by the ERC advanced grant GA 339899-EDIFICE under the ERC's 7th Framework Program (FP7-IDEA-ERC). The data presented in this study are available within the Supplementary Material or upon requested to simon@cerege.fr.

Appendix A. Supplementary material

Supplementary material related to this article can be found online at https://doi.org/10.1016/j.epsl.2017.11.021.

References

Balbas, A., Koppers, A.A.P., Kent, D.V., Konrad, K., Clark, P.U., 2016. Identification of the short-lived Santa Rosa geomagnetic excursion in lavas on Floreana Island (Galapagos) by $^{40}Ar/^{39}Ar$ geochronology. Geology 44 (5), 359–362. https://doi.org/10.1130/g37569.1. G37569.1.

Beer, J., Mccracken, K., von Steiger, R., 2012. Cosmogenic Radionuclides: Theory and Applications in Terrestrial and Space Environments. Physics of Earth and Space Environments. Springer-Verlag, Berlin. 428 pp.

Biggin, A.J., Strik, G., Langereis, C.G., 2009. The intensity of the geomagnetic field in the late-Archaean: new measurements and an analysis of the updated IAGA palaeointensity database. Earth Planets Space 61 (1), 9–22.

Bourlès, D.L., Raisbeck, G.M., Yiou, F., 1989. ^{10}Be and ^{9}Be in Marine sediments and their potential for dating. Geochim. Cosmochim. Acta 53 (2), 443–452.

Braucher, R., Guillou, V., Bourlès, D.L., Arnold, M., Aumaître, G., Keddadouche, K., Nottoli, E., 2015. Preparation of ASTER in-house $^{10}Be/^{9}Be$ standard solutions. Nucl. Instrum. Methods Phys. Res., Sect. B, Beam Interact. Mater. Atoms 361, 335–340. https://doi.org/10.1016/j.nimb.2015.06.012.

Brown, M.C., Donadini, F., Nilsson, A., Panovska, S., Frank, U., Korhonen, K., Schuberth, Korte, M., Constable, C.G., 2015. GEOMAGIA50.v3: 2. A new paleomagnetic database for lake and marine sediments. Earth Planets Space 67–70. https://doi.org/10.1186/s40623-015-0233-z.

Carcaillet, J.T., Thouveny, N., Bourlès, D.L., 2003. Geomagnetic moment instability between 0.6 and 1.3 Ma from cosmonuclide evidence. Geophys. Res. Lett. 30 (15), 1792. https://doi.org/10.1029/2003GL017550.

Carcaillet, J.T., Bourlès, D.L., Thouveny, N., 2004. Geomagnetic dipole moment and ^{10}Be production rate intercalibration from authigenic $^{10}Be/^{9}Be$ for the last 1.3 Ma. Geochem. Geophys. Geosyst. 5 (5), Q05006. https://doi.org/10.1029/2003GC000641.

Channell, J.E.T., Mazaud, A., Sullivan, P., Turner, S., Raymo, M.E., 2002. Geomagnetic excursions and paleointensities in the Matuyama Chron at Ocean Drilling Program Sites 983 and 984 (Iceland Basin). J. Geophys. Res. 107 (B6). https://doi.org/10.1029/2001JB000491.

Channell, J.E.T., Labs, J., Raymo, M.E., 2003. The Réunion subchronozone at ODP Site 981 (Feni Drift, North Atlantic). Earth Planet. Sci. Lett. 215, 1–12.

Channell, J.E.T., Xuan, C., Hodell, D.A., 2009. Stacking paleointensity and oxygen isotope data for the last 1.5 Myr (PISO-1500). Earth Planet. Sci. Lett. 283 (1–4), 14–23. https://doi.org/10.1016/j.epsl.2009.03.012.

Channell, J.E.T., Hodell, D.A., Singer, B.S., Xuan, C., 2010. Reconciling astrochronological and $^{40}Ar/^{39}Ar$ ages for the Matuyama–Brunhes boundary in the late Matuyama Chron. Geochem. Geophys. Geosyst. 11, Q0AA12. https://doi.org/10.1029/2010GC003203.

Channell, J.E.T., Hodell, D.A., Curtis, J.H., 2016. Relative paleointensity (RPI) and oxygen isotope stratigraphy at IODP Site U1308: North Atlantic RPI stack for 1.2–2.2 Ma (NARPI-2200) and age of the Olduvai Subchron. Quat. Sci. Rev. 131, 1–19.

Channell, J.E.T., 2017. Magnetic excursions in the late Matuyama Chron (Olduvai to Matuyama–Brunhes boundary) from North Atlantic IODP sites. J. Geophys. Res., Solid Earth 122. https://doi.org/10.1002/2016JB013616.

Chmeleff, J., von Blanckenburg, F., Kossert, K., Jakob, D., 2010. Determination of the ^{10}Be half-life by multicollector ICP-MS and liquid scintillation counting. Nucl. Instrum. Methods Phys. Res. B 268 (2), 192–199. https://doi.org/10.1016/j.nimb.2009.09.012.

Christl, M., Lippold, J., Steinhilber, F., Bernsdorff, F., Mangini, A., 2010. Reconstruction of global ^{10}Be production over the past 250 ka from highly accumulating Atlantic drift sediments. Quat. Sci. Rev. 29 (19–20), 2663–2672. https://doi.org/10.1016/j.quascirev.2010.06.017.

Coe, R.S., Singer, B.S., Pringle, M.S., Zhao, X., 2004. Matuyama–Brunhes reversal and Kamikatsura event on Maui: paleomagnetic directions, $^{40}Ar/^{39}Ar$ ages and implications. Earth Planet. Sci. Lett. 222, 667–684.

Cohen, K.M., Gibbard, P.L., 2016. Global Chronostratigraphical Correlation Table for the Last 2.7 Million Years v.2016a. Subcommission on Quaternary Stratigraphy, International Commission on Stratigraphy, Cambridge.

de Garidel-Thoron, T., Rosenthal, Y., Bassinot, F., Beaufort, L., 2005. Stable sea surface temperatures in the western Pacific warm pool over the past 1.75 million years. Nature 433, 294–298.

Frank, M., Schwarz, B., Baumann, S., Kubik, P.W., Suter, M., Mangini, A., 1997. A 200 kyr record of cosmogenic radionuclide production rate and geomagnetic field intensity from ^{10}Be in globally stacked deep-sea sediments. Earth Planet. Sci. Lett. 149 (1–4), 121–129.

Glatzmaier, G.A., Coe, R.S., 2015. Magnetic polarity reversals in the core. In: Treatise on Geophysics, vol. 8, Geomagnetism, second edition. Elsevier, Amsterdam, pp. 279–295 (Chapter 11).

Guyodo, Y., Richter, C., Valet, J.P., 1999. Paleointensity record from Pleistocene sediments (1.4–0 Ma) off the California Margin. J. Geophys. Res., Solid Earth 104 (B10), 22953–22964. https://doi.org/10.1029/1999JB900163.

Hagstrum, J.T., Fleck, R.J., Evarts, R.C., Calvert, A.T., 2017. Paleomagnetism and $^{40}Ar/^{39}Ar$ geochronology of the Plio-Pleistocene Boring Volcanic Field: implications for the geomagnetic polarity time scale and paleosecular variation. Phys. Earth Planet. Inter. 262, 101–115.

Hartl, P., Tauxe, L., 1996. A precursor to the Matuyama/Brunhes transition-field instability as recorded in pelagic sediments. Earth Planet. Sci. Lett. 138, 121–135.

Horng, C.S., Lee, M.Y., Palike, H., Wei, K.Y., Liang, W.T., Iizuka, Y., Torii, M., 2002. Astronomically calibrated ages for geomagnetic reversals within the Matuyama chron. Earth Planets Space 54, 679–690.

Horng, C.S., Roberts, A.P., Liang, W.T., 2003. A 2.14-Myr astronomically tuned record of relative geomagnetic paleointensity from the western Philippine Sea. J. Geophys. Res. 108 (B11), 2059. https://doi.org/10.1029/2001JB001698.

Kissel, C., Guillou, H., Laj, C., Carracedo, J.C., Perez-Torrado, F., Wandres, C., Rodriguez-Gonzalez, A., Nomade, S., 2014. A combined paleomagnetic/dating investigation of the upper Jaramillo transition from a volcanic section at Tenerife (Canary Islands). Earth Planet. Sci. Lett. 406, 59–71.

Knudsen, M.F., Henderson, G.M., Frank, M., Mac Niocaill, C., Kubik, P.W., 2008. In-phase anomalies in beryllium-10 production and palaeomagnetic field behaviour during the Iceland Basin geomagnetic excursion. Earth Planet. Sci. Lett. 265 (3–4), 588–599. https://doi.org/10.1016/j.epsl.2007.10.051.

Korschinek, G., Bergmaier, A., Faestermann, T., Gerstmann, U.C., Knie, K., Rugel, G., Wallner, A., Dillmann, I., Dollinger, G., Lierse von Gostomski, Ch., Kossert, K., Maiti, M., Poutivtsev, M., Remmert, A., 2010. A new value for the half-life of ^{10}Be by Heavy-Ion Elastic Recoil Detection and liquid scintillation counting. Nucl. Instrum. Methods Phys. Res. B 268 (2), 187–191. https://doi.org/10.1016/j.nimb.2009.09.020.

Laj, C., Channell, J.E.T., 2015. Geomagnetic excursions. In: Treatise on Geophysics, vol. 5, Geomagnetism, second edition. Elsevier, Amsterdam, pp. 343–383 (Chapter 10).

Laskar, J., Joutel, F., Boudin, F., 1993. Orbital, precessional, and insolation quantities for the earth from −20 Myr to +10 Myr. Astron. Astrophys. 270, 522–533.

Laskar, J., Robutel, P., Joutel, F., Gastineau, M., Correia, A.C.M., Levrard, B., 2004. A long termnumerical solution for the insolation quantities of the Earth. Astron. Astrophys. 428, 261–285. https://doi.org/10.1051/0004-6361:20041335.

Lee, M.Y., Wei, K.Y., 2000. Australasian microtektites in the South China Sea and the West Philippine Sea: implications for age, size and location of the impact crater. Meteorit. Planet. Sci. 35, 1151–1156.

Lisiecki, L.E., Raymo, M.E., 2005. A Pliocene–Pleistocene stack of 57 globally distributed benthic $\delta^{18}O$ record. Paleoceanography 20, 1–17. https://doi.org/10.1029/2004PA001071.

Lisiecki, L.E., Raymo, M.E., 2009. Diachronous benthic $\delta^{18}O$ responses during late Pleistocene terminations. Paleoceanography 24, PA3210. https://doi.org/10.1029/2009PA001732.

Lourens, L.J., 2004. Revised tuning of Ocean Drilling Program Site 964 and KC01B (Mediterranean) and implications for the ^{18}O, tephra, calcareous nannofossil, and geomagnetic reversal chronologies of the past 1.1 Myr. Paleoceanography 19, PA3010.

Mark, D.F., Renne, P.R., Dymock, R., Smith, V.C., Simon, J.I., Morgan, L.E., Staff, R.A., Ellis, B.S., 2017. High-precision $^{40}Ar/^{39}Ar$ dating of pleistocene tuffs and temporal anchoring of the Matuyama–Brunhes boundary. Quat. Geochronol. 39, 1–23.

Masarik, J., Beer, J., 2009. An updated simulation of particle fluxes and cosmogenic nuclide production in the Earth's atmosphere. J. Geophys. Res. 114, D11103. https://doi.org/10.1029/2008JD010557.

Mazaud, A., Channell, J.E.T., Stoner, J.S., 2012. Relative paleointensity and environmental magnetism since 1.2 Ma at IODP Site U1305 (Eirik Drift, NW Atlantic). Earth Planet. Sci. Lett. 357–358, 137–144.

Ménabréaz, L., Bourlès, D.L., Thouveny, N., 2012. Amplitude and timing of the Laschamp geomagnetic dipole low from the global atmospheric ^{10}Be overproduction: contribution of authigenic $^{10}Be/^{9}Be$ ratios in west equatorial Pacific sediments. J. Geophys. Res. 117 (B11101). https://doi.org/10.1029/2012JB009256.

Ménabréaz, L., Thouveny, N., Bourlès, D.L., Vidal, L., 2014. The geomagnetic dipole moment variation between 250 and 800 ka BP reconstructed from the authigenic $^{10}Be/^{9}Be$ signature in West Equatorial Pacific sediments. Earth Planet. Sci. Lett. 385, 190–205. https://doi.org/10.1016/j.epsl.2013.10.037.

Nomade, S., Bassinot, F., Marino, M., Dewilde, D., Maiorano, P., Esguder, G., Blamart, D., Girone, A., Scao, V., Pereira, A., Toti, F., Bertini, A., Simon, Q., Combourieu-Nebout, N., Peral, M., Bourlès, D.L., Petrosino, P., Ciaranfi, N., in prep. High-resolution foraminifer stable isotope record of MIS 19 at Montalbano Jonico, southern Italy: a window into Mediterranean climatic variability during a low-eccentricity interglacial.

Ogg, J.G., 2012. The geomagnetic polarity timescale. In: Gradstein, F., Ogg, J.G., Schmitz, M., Ogg, G. (Eds.), The Geologic Time Scale 2012. Elsevier, Amsterdam, pp. 85–128.

Okada, M., Suganuma, Y., Haneda, Y., Kazaoka, O., 2017. Paleomagnetic direction and paleointensity variations during the Matuyama–Brunhes polarity transition from a marine succession in the Chiba composite section of the Boso Peninsula, central Japan. Earth Planets Space 69, 45. https://doi.org/10.1186/s40623-017-0627-1.

Olson, P.L., Coe, R.S., Driscoll, P.E., Glatzmaier, G.A., Roberts, P.H., 2010. Geodynamo reversal frequency and heterogeneous core–mantle boundary heat flow. Phys. Earth Planet. Inter. 180, 66–79.

Petrosino, P., Jicha, B.R., Mazzeo, F.C., Ciaranfi, N., Girone, A., Maiorano, P., Marino, M., 2015. The Montalbano Jonico marine succession: an archive for distal tephra layers at the Early–Middle Pleistocene boundary in southern Italy. Quat. Int. 383, 89–103.

Raisbeck, G.M., Yiou, F., Cattani, O., Jouzel, J., 2006. ^{10}Be evidence for the Matuyama–Brunhes geomagnetic reversal in the EPICA Dome C ice core. Nature 444 (7115), 82–84. https://doi.org/10.1038/nature05266.

Roberts, A.P., Winklhofer, M., 2004. Why are geomagnetic excursions not always recorded in sediments? Constraints from post-depositional remanent magnetization lock-in modelling. Earth Planet. Sci. Lett. 227, 345–359.

Roberts, A.P., Tauxe, L., Heslop, D., 2013. Magnetic paleointensity stratigraphy and high-resolution Quaternary geochronology: successes and future challenges. Quat. Sci. Rev. 61, 1–16.

Roger, S., Coulon, C., Thouveny, N., Féraud, G., Van Velzen, A., Fauquette, S., Cochemé, J.J., Prévot, M., Verosub, K.L., 2000. ^{40}Ar/^{39}Ar dating of a tephra layer in the Pliocene Senéze maar lacustrine sequence (French Massif Central): constraint on the age of the Réunion—Matuyama transition and implications on paleoenvironmental archives. Earth Planet. Sci. Lett. 183 (3–4), 431–440.

Simon, Q., Thouveny, N., Bourlès, D.L., Nuttin, L., Hillaire-Marcel, C., St-Onge, G., 2016b. Authigenic ^{10}Be/^{9}Be ratios and ^{10}Be-fluxes (^{230}Th$_{xs}$-normalized) in central Baffin Bay sediments during the last glacial cycle: paleoenvironmental implications. Quat. Sci. Rev. 140, 142–162. https://doi.org/10.1016/j.quascirev.2016.03.027.

Simon, Q., Thouveny, N., Bourlès, D.L., Valet, J.P., Bassinot, F., Ménabréaz, L., Guillou, V., Choy, S., Beaufort, L., 2016a. Authigenic ^{10}Be/^{9}Be ratio signatures of the cosmogenic nuclide production linked to geomagnetic dipole moment variation since the Brunhes/Matuyama boundary. J. Geophys. Res., Solid Earth 121. https://doi.org/10.1002/2016JB013335.

Simon, Q., Bourlès, D.L., Bassinot, F., Nomade, S., Marino, M., Ciaranfi, N., Girone, A., Maiorano, P., Thouveny, N., Choy, S., Dewilde, F., Scao, V., Isguder, G., Blamart, D., ASTER Team, 2017. Authigenic ^{10}Be/^{9}Be ratio signature of the Matuyama–Brunhes boundary in the Montalbano Jonico marine succession. Earth Planet. Sci. Lett. 460, 255–267. https://doi.org/10.1016/j.epsl.2016.11.052.

Singer, B.S., Hoffman, K.A., Chauvin, A., Coe, R.S., Pringle, M.S., 1999. Dating transitionally magnetized lavas of the late Matuyama chron: toward a new ^{40}Ar/^{39}Ar timescale of reversals and events. J. Geophys. Res. 104, 679–693.

Singer, B.S., 2014. A quaternary geomagnetic instability time scale. Quat. Geochronol. 21, 29–52.

Singer, B.S., Jicha, B.R., Mochizuki, N., Coe, R.S., 2017. ^{40}Ar/^{39}Ar multi-collector revolution and age of the Matuyama–Brunhes boundary. In: GSA Annual Meeting in Seattle. Washington, USA, Paper No. 352-4.

Shackleton, N.J., 1974. Attainment of isotopic equilibrium between ocean water and the benthonic foraminiferal genus Uvigerina: isotopic changes in the ocean during the last glacial. Cent. Natl. Rech. Sci. Colloq. Int. 219, 203–209.

Suganuma, Y., Yokoyama, Y., Yamazaki, T., Kawamura, K., Horng, C.-S., Matsuzaki, H., 2010. ^{10}Be evidence for delayed acquisition of remanent magnetization in marine sediments: implication for a new age for the Matuyama–Brunhes boundary. Earth Planet. Sci. Lett. 296, 443–450. https://doi.org/10.1016/j.epsl.2010.05.031.

Suganuma, Y., Okuno, J., Heslop, D., Roberts, A.P., Yamazaki, T., Yokoyama, Y., 2011. Post-depositional remanent magnetization lock-in for marine sediments deduced from ^{10}Be and paleomagnetic records through the Matuyama–Brunhes boundary. Earth Planet. Sci. Lett. 311, 39–52.

Suganuma, Y., Okada, M., Horie, K., Kaiden, H., Takehara, M., Senda, R., Kimura, J.-I., Kawamura, K., Haneda, Y., Kazaoka, O., Head, M.J., 2015. Age of Matuyama–Brunhes boundary constrained by U–Pb zircon dating of a widespread tephra. Geology 43, 491–494. https://doi.org/10.1130/G36625.1.

Tauxe, L., Herbert, T., Shackleton, N.J., Kok, Y.S., 1996. Astronomical calibration of the Matuyama–Brunhes boundary: consequences for magnetic remanence acquisition in marine carbonates and the Asian loess sequences. Earth Planet. Sci. Lett. 140, 133–146.

Thouveny, N., Bourlès, D.L., Saracco, G., Carcaillet, J., Bassinot, F., 2008. Paleoclimatic context of geomagnetic dipole lows and excursions in the Brunhes, clue for an orbital influence on the geodynamo? Earth Planet. Sci. Lett. 275, 269–284.

Valet, J.P., Meynadier, L., Guyodo, Y., 2005. Geomagnetic field strength and reversal rate over the past 2 million years. Nature 435, 802–805.

Valet, J.P., Bassinot, F., Bouilloux, A., Bourlès, D.L., Nomade, S., Guillou, V., Lopes, F., Thouveny, N., Dewilde, F., 2014. Geomagnetic, cosmogenic and climatic changes across the last geomagnetic reversal from Equatorial Indian Ocean sediments. Earth Planet. Sci. Lett. 397, 67–79. https://doi.org/10.1016/j.epsl.2014.03.053.

Valet, J.P., Meynadier, L., Simon, Q., Thouveny, N., 2016. When and why sediments fail to record the geomagnetic field during polarity reversals? Earth Planet. Sci. Lett. 453, 96–107.

Valet, J.P., Fournier, A., 2016. Deciphering records of geomagnetic reversals. Rev. Geophys. 54. https://doi.org/10.1002/2015RG000506.

von Blanckenburg, F., Igel, H., 1999. Lateral mixing and advection of reactive isotope tracers in ocean basins: observations and mechanisms. Earth Planet. Sci. Lett. 169, 113–128.

Xuan, C., Channell, J.E.T., Hodell, D.A., 2016. Quaternary magnetic and oxygen isotope stratigraphy in diatom-rich sediments of the southern Gardar Drift (IODP Site U1304, North Atlantic). Quat. Sci. Rev. 142, 74–89.

Yamazaki, T., Oda, H., 2005. A geomagnetic paleointensity stack between 0.8 and 3.0 Ma from equatorial Pacific sediment cores. Geochem. Geophys. Geosyst. 6, Q11H20. https://doi.org/10.1029/2005GC001001.

Zhou, W., Beck, W., Kong, X., An, Z., Qiang, X., Wu, Z., Xian, F., Ao, H., 2014. Timing of the Brunhes–Matuyama magnetic polarity reversal in Chinese loess using ^{10}Be. Geology 42 (6), 467–470. https://doi.org/10.1130/G35443.1.

Ziegler, L.B., Constable, C.G., Johnson, C.L., Tauxe, L., 2011. PADM2M: a penalized maximum likelihood model of the 0–2 Ma palaeomagnetic axial dipole moment. Geophys. J. Int. 184, 1069–1089. https://doi.org/10.1111/j.1365-246X.2010.04905.x.